Depletion of eukaryotic initiation factor 5B (eIF5B) reprograms the cellular transcriptome and leads to activation of endoplasmic reticulum (ER) stress and c-Jun N-terminal Kinase (JNK).

Kamiko R. Bressler [1, †, ^], Joseph A. Ross [1, †, ‡], Slava Ilnytskyy [2, †], Keiran Vanden Dungen [1], Katrina Taylor [1], Kush Patel [1], Athanasios Zovoilis[1,3,5], Igor Kovalchuk [2,5], and Nehal Thakor [1,2,3,4,5*]

[1]Department of Chemistry and Biochemistry, University of Lethbridge, 4401 University Drive W, Lethbridge, Alberta, T1K 3M4, Canada.

[2] Department of Biological Sciences, University of Lethbridge, 4401 University Drive W, Lethbridge, Alberta, T1K 3M4, Canada.

[3] Canadian Centre for Behavioral Neuroscience (CCBN), Department of Neuroscience, University of Lethbridge, 4401 University Drive W, Lethbridge, Alberta, T1K 3M4, Canada.

[4]Arnie Charbonneau Cancer Institute, Cumming School of Medicine, University of Calgary, 3280 Hospital Drive NW, Calgary, Alberta, T2N 4Z6, Canada

[5] Southern Alberta Genome Sciences Centre (SAGSC), University of Lethbridge, 4401 University Drive W, Lethbridge, Alberta, T1K 3M4, Canada.

[†] These authors contributed equally to this work

[^] Current affiliation: MD candidate, Cumming School of Medicine, University of Calgary, 3280 Hospital Drive NW, Calgary, Alberta, T2N 4Z6, Canada

[‡] Current affiliation: Senior Scientist, Chinook Contract Research Inc., 97 East Lake Ramp NE, Airdrie, Alberta, T4A 2K4, Canada

***** Correspondence: nthakor@uleth.ca; Tel.: +1-403-317-5055

Keywords: Eukaryotic initiation factor 5B (eIF5B), ER stress, transcriptome, ISR, ATF4, JNK

Running title: Depletion of eIF5B reprograms cellular transcriptome

Abstract: During the integrated stress response (ISR) global translation initiation is attenuated; however, non-canonical mechanisms allow for the continued translation of specific transcripts. Eukaryotic initiation factor 5B (eIF5B) has been shown to play a critical role in canonical translation as well as in non-canonical mechanisms involving internal ribosome entry site (IRES) and upstream open reading frame (uORF) elements. The uORF-mediated translation regulation of *activating transcription factor 4* (*ATF4)* mRNA plays a pivotal role in the cellular ISR. Our recent study confirmed that eIF5B depletion removes uORF2-mediated repression of *ATF4* translation, which results in the upregulation of *Growth arrest and DNA damage-inducible protein 34 (GADD34)* transcription. Accordingly, we hypothesized that eIF5B depletion may reprogram the transcriptome profile of the cell. Here, we employed genome-wide transcriptional analysis on eIF5B-depleted cells. Further, we validate the up- and down-regulation of several transcripts from our RNA-seq data using RT-qPCR. We identified upregulated pathways including cellular response to endoplasmic reticulum (ER) stress, and mucin-type O-glycan biosynthesis, as well as downregulated pathways of transcriptional misregulation in cancer, and T-cell receptor signaling. We also confirm that depletion of eIF5B leads to activation of the c-jun N-terminal kinase (JNK) arm of the mitogen-activated protein kinase (MAPK) pathway. This data suggests that depletion of eIF5B reprograms the cellular transcriptome and influences critical cellular processes such as ER stress and ISR.

Introduction

Translation is a complex process involving at least twelve initiation factors and is tightly regulated—particularly at initiation, which is the rate-limiting step (Graber and Holcik 2007). Dysregulation of protein synthesis can result in diseases, including cancer. In response to stress conditions such as hypoxia, nutrient starvation, or endoplasmic reticulum (ER) stress, one of four kinases are activated: PKR-like ER kinase (PERK), protein kinase double stranded RNA-dependent (PKR), heme-regulated inhibitor (HRI), and general control non-derepressible-2 (GCN2). Each of these kinases phosphorylate the alpha (α) subunit of eIF2 at serine 51 (Pakos-Zebrucka et al. 2016). This phosphorylation blocks the eIF2B-mediated exchange of GDP for GTP which consequently prevents the formation of the ternary complex (Starck et al. 2016). The ternary complex is required to deliver initiator-tRNA to the ribosomal complex to form the 43S pre-initiation complex. Thus,

global translation initiation is attenuated during stress conditions. However, specific transcripts involved in adaptation to stress, such as *activating transcription factor 4* (*ATF4)*, are translated through non-canonical mechanisms under these conditions (Dey et al. 2010).

The cis-acting RNA elements, such as upstream open reading frames (uORFs) and internal ribosome entry sites (IRESs) often promote the translation of mRNAs involved in the stress response, cell cycle regulation, cell survival, and cell death (Calvo et al. 2009). IRES- and uORF-mediated translation mechanisms differ from canonical translation initiation in that they can operate under conditions of limited availability of ternary complex (Sharma et al. 2016). Importantly, however, these mechanisms still rely on the delivery of initiator-tRNA. In canonical translation initiation, delivery of initiator-tRNA is mediated by the ternary complex, consisting of eIF2–initiator-tRNA–GTP (Holcik and Sonenberg 2005). The eukaryotic homologue of bacterial IF2, which delivers initiator-tRNA^{fmet} in bacteria, is eIF5B. The role of eIF5B in canonical translation initiation is to promote 60S ribosome subunit joining and pre-40S subunit proofreading (Sharma et al. 2016). However, eIF5B has been confirmed to directly interact with initiator-tRNA (Lee et al. 2014). Further, it has been shown that eIF5B can parallel eIF2's tRNA delivery role in the IRES-dependent translation of the mRNAs of *classical swine fever virus* (*CSFV*) and *hepatitis C virus* (*HCV)*, as well as the cellular mRNA encoding *X-linked inhibitor of apoptosis protein* (*XIAP*) (Pestova et al. 2008; Terenin et al. 2008; Thakor and Holcik 2012). Moreover, eIF5B was recently shown to deliver initiator-tRNA under hypoxic stress conditions (Ho et al. 2018), and we have shown that eIF5B regulates the translation of a group of IRES-containing mRNAs encoding anti-apoptotic and pro-survival proteins in U343 glioblastoma cells (Ross et al. 2019). We also recently determined that eIF5B represses the uORF-dependent translation of *ATF4*, which is a master transcription factor controlling the ISR pathway (Ross et al. 2018). Further, depletion of eIF5B derepressed the uORF2-mediated translation repression of *ATF4* mRNA (Ross et al. 2018). As a natural advancement of our previous study, we analyzed changes in the cellular transcriptome upon eIF5B depletion. Indeed, we show that silencing eIF5B by RNAi results in reprogramming of the cellular transcriptome, resulting in several significantly upregulated and downregulated pathways. RT-qPCR validates the top three upregulated and top three downregulated transcripts from the transcriptome analysis. The MAPK/JNK axis is activated upon depletion of eIF5B, and we specifically verify activation of JNK.

As JNK is one of the three major groups of MAP kinases—along with classical extracellular signal-regulated kinase (ERK) and p38—we suggest that eIF5B depletion regulates the complex MAPK signaling pathway *via* JNK activation. Moreover, we also show that the depletion of eIF5B leads to the activation of ER stress as revealed by enhanced expression of CHOP, GADD34, and XBP1. Here we demonstrate that although eIF5B is a translation initiation factor it is indirectly involved in regulating cellular transcriptome. We also implicate eIF5B in regulating ER stress via modulating the expression of ER-stress related proteins.

Methods

Cell culture and reagents

HEK 293T cells were purchased from the American Type Culture Collection (ATCC). HEK 293T were propagated in Dulbecco's high modified Eagle's medium (DMEM; HyClone) with 4 mM L-glutamine, 4500 mg/L glucose, and 1 mM sodium pyruvate, supplemented with 10% fetal bovine serum (FBS; Gibco) and 1% penicillin-streptomycin (Gibco). Cells were incubated at 37 ºC in a humidified incubator at 5% CO_2. Cell lines were routinely tested for mycoplasma contamination with a PCR mycoplasma detection kit (ABM). Reverse transfections were carried out using Lipofectamine RNAiMAX (Invitrogen) according to the manufacturer's instructions. Non-specific control siRNA (siC) was obtained from Qiagen. Stealth RNAi^{TM} siRNAs targeting eIF5B (HSS114469/70/71) were obtained from Invitrogen.

RNA Isolation

HEK 293T cells were seeded at 200,000 cells/well and reverse-transfected in 6-well plates. After 96 hours, RNA was isolated essentially as described (Faye et al. 2014) except that proteinase K treatment was replaced by incubation with 1% SDS at 65ºC for 1 min, and hot acid phenol:chloroform (5:1; Ambion) was used to extract the RNA.

RNA-seq Data Analysis

Data analysis and sequencing was performed using the Illumina NextSeq500 platform, with 75 bp single-end configuration. The Illumina TruSeq Stranded mRNA (polyA-selection) kit was used for library construction according to the manufacturer's instructions. The reference genome (Human

GRCh37 Ensembl) was downloaded from Illumina iGENOME, and base-calling and de-multiplexing were done using the Illumina CASAVA 1.9 pipeline.

Upon initial sequencing, the library quality control was conducted with FastQC 0.11.5. Reads (Supplemental Table S1 for number of reads) were then mapped to the human genome (Ensembl, GRCh37) using hisat2, version 2.0.5 (Kim et al. 2015). SAM files generated by hisat2 were converted to BAM, sorted, and indexed using samtools 1.7 (Czeh and Czopf 1991). Reads mapping to genes were counted using featureCounts, version 1.6.1 (Liao et al. 2014). Differentially expressed genes were detected using DESeq2 1.18.1 Bioconductor package (Love et al. 2014). Genes with adjusted p-values (Bonferroni-Hochberg adjustment for multiple comparisons) less than 0.05, and over a 2-fold change in magnitude, were selected as differentially expressed (430 upregulated and 216 downregulated). Over-represented gene ontology (GO) terms were detected using the function annotation module of the DAVID platform applying default parameters (Huang da et al. 2009a; Huang da et al. 2009b). GO analysis was conducted separately on up-, down-, and all differentially-expressed genes. Over-representation analysis of KEGG pathways was performed using the same platform with pathway data obtained from the Kyoto Encyclopedia of Genes and Genomes (KEGG) (Kanehisa and Goto 2000). Similarly to GO analysis, over-represented pathways were detected separately for up-, down-, and all differentially-expressed genes.

RT-qPCR

RT-qPCR was performed using RNA samples obtained from the independent set of transfection experiments and not from the RNA samples obtained for RNAseq experiments. RNA was isolated using a New England Biolabs Monarch Total RNA Miniprep kit, and cDNA was generated from equal volumes of RNA using the qScript cDNA synthesis kit (Quanta Biosciences). Quantitative PCR was performed in a CFX-96 real-time thermocycler (Bio-Rad) with PerfeCTa SYBR Green SuperMix (Quanta Biosciences) according to the manufacturer's instructions. Primers (Quantitect Primer Assays) were obtained from Qiagen (KLHDC7B, QT00208117; WFIKKN2, QT00213948; OLFML1, QT00074620; KCNJ10, QT00059031; SEZ6, QT01030232; SYT4, QT00003269). Negative controls without template DNA were run in duplicate. Each reaction was run in triplicate with the following cycle conditions: 1 cycle at 95°C for 3 min followed by 45 cycles of 95°C for 15

s, 55°C for 35 s, and 72°C for 1 min. A melting curve step was added to check the purity of the PCR product. This step consisted of a ramp of the temperature from 65 to 95°C at an increment of 0.5°C and a hold for 5 seconds at each step. Amplicons were quantified by the ΔΔCt method.

Western blotting

HEK 293T cells were seeded at 200,000 cells/well and reverse-transfected in 6-well plates. After 96 hours, cells were harvested in RIPA lysis buffer supplemented with protease inhibitors. Equal amounts of soluble protein (typically 20 µg per well) were resolved by SDS-PAGE and transferred onto nitrocellulose membranes (GE healthcare). Individual proteins were detected by immunoblotting with the antibodies listed in Supplemental Table S4. Actin was detected using fluorescently labeled primary antibody (hFAB Rhodamine). All other primary antibodies were detected with anti-rabbit-HRP conjugate (Abcam) in an AI600 imager (GE) and densitometry performed using the AI600 analysis software.

Statistical analyses for RT-qPCR and Western blots

Unless otherwise specified, all quantitative data represent the mean ± standard error on the mean (SEM) for at least 3 independent biological replicates. Statistical significance was determined by an unpaired, two-tailed t-test without assuming equal variance. The significance level was set at a p-value of 0.05. Data was analyzed using GraphPad Prism, version 7.

Results

eIF5B depletion results in transcriptome-wide changes in signaling pathways

To investigate the impact of eIF5B upon the transcriptome, eIF5B was depleted from HEK 293T cells using siRNA (Figure 1A) and transcriptional profiles were analyzed by RNAseq. Depletion of eIF5B was confirmed to result in significant transcriptome-wide changes. The volcano plot (Figure 1B) shows significantly ($p<0.05$) differentially expressed genes (DEGs) (in blue) upon eIF5B depletion. The heatmap (Figure 1C) shows all DEGs with an adjusted p-value <0.05 and log2 fold change over 1 between eIF5B-depleted and control HEK 293T samples (red, upregulated; green, downregulated). A complete list of genes with a significantly altered expression upon eIF5B depletion

is presented in Supplemental Table S1, S2 and S3. Analysis of biochemical pathways was performed and significantly upregulated and downregulated genes were sorted into biologically relevant signaling pathways (Table 1, Table 2, Supplemental Table S1, S2 & S3, and Supplemental Figure S1). Pathways that were significantly upregulated were mucin type O-glycan biosynthesis, neuroactive ligand-receptor interactions, protein processing in the ER (ISR genes; *growth arrest and DNA damage-inducible protein 34* (*GADD34)* and *C/EBP homologous protein (CHOP)*), and the synaptic vesicle cycle (Table 1). Pathways that were significantly downregulated were transcriptional misregulation in cancer, and human T0Lymphotropic Virus Type 1 (HTLV-I) infection (Table 2).

Validation of transcriptome profile

Previously, we have shown that eIF5B depletion enhances the translation of *ATF4* mRNA and as a result the levels of *GADD34* mRNA and protein increases.(Ross et al. 2018) Here also we show that *GADD34* expression is enhanced in eIF5B-depleted HEK293T cells without an increase in *ATF4* mRNA (Supplemental Fig. 1 and Supplemental Table S1 & S2). To further validate the transcriptome analysis, we employed RT-qPCR to quantify the three most upregulated and three most downregulated genes upon eIF5B depletion. The three most upregulated transcripts observed in our transcriptome profile upon silencing eIF5B were *kelch domain containing 7B* (*KLHDC7B*) ($2^{7.68}$), *seizure related 6 homolog* (*SEZ6*) ($2^{7.39}$), and *synaptotagmin 4* (*SYT4*) ($2^{6.95}$) (Supplemental Table S1). The three most downregulated genes were *potassium voltage-gated channel subfamily J member 10* (*KCNJ10*) ($2^{-5.25}$), *WAP Follistatin/Kazal Immunoglobulin Kunitz and Netrin domain containing 2* (*WFIKKN2*) ($2^{-4.43}$), and *olfactomedin like 1* (*OLFML1*) ($2^{-4.18}$) (Supplemental Table S1). Following RT-qPCR analysis, we found that the six genes were significantly regulated as expected, ensuring the validity of our transcriptome data (Figure 2).

ER stress and JNK activation are closely linked with each other (Darling and Cook 2014; Raciti et al. 2012). We observed that several ER stress-related genes, such as *DDIT3, XBP*, and *GADD34* are differentially expressed in eIF5B-depleted cells (Supplemental Table S1). Moreover, we show here that genes involved in JNK/C-jun/AP-1 axis, such as *basic leucine zipper ATF-like transcription factor 3* (*BATF3), CD9, dickkopf-related protein 3 (DKK3)*, *platelet derived growth factor subunit A (PDGFA)*, and *ancient ubiquitous protein 1* (*AUP1)*, are differentially expressed in eIF5B-depleted

cells (Table 3). Therefore, we hypothesized that JNK would be activated along with ER stress in eIF5B depleted cells. Indeed, eIF5B depletion in HEK 293T cells resulted in enhanced levels of phosphorylated JNK (~ 2-fold), despite a significant decrease in overall JNK levels (Figure 3 and Supplemental Figure S2). This confirms that, although less JNK is present in cells depleted of eIF5B, the JNK is being activated at higher levels. Despite enhanced levels of phosphorylated JNK, we observed modestly decreased levels of HSF1 and decreased levels of phosphorylated HSF1 (Figure 3 and Supplemental Figure S2). Additionally, we have observed upregulation of CHOP, GADD34, and XBP1 proteins in eIF5B-depleted cells (Figure 3 and Supplemental Figure S2). We have also observed decreased levels of BiP protein in eIF5B-depleted cells (Figure 3 and Supplemental Figure S2). This validates the changes we observed in transcriptome profile affected by the levels of eIF5B.

Discussion

In this work, we confirm that the depletion of eIF5B leads to massive reprograming of the cellular transcriptome, resulting in significant changes in multiple signaling pathways. We validate our transcriptome data by performing RT-qPCR on the top upregulated and downregulated transcripts (Figure 2). Additionally, we verified that the ER stress and JNK-arm of the MAPK signaling pathway are activated upon depletion of eIF5B. This work offers new insight into the potential role of eIF5B as a regulatory hub.

We observed that, upon eIF5B depletion, the cellular transcriptome was robustly reprogrammed (Figure 1). A number of pathways were shown to be significantly upregulated, specifically mucin-type O-glycan biosynthesis, neuroactive ligand-receptor interactions, protein processing in the ER, and the synaptic vesicle cycle (Table 1, Supplemental Figure 1). Pathways that were significantly downregulated were transcriptional misregulation in cancer, and T-cell receptor signaling (Table 2, Supplemental Figure 1).

Under stress conditions, phosphorylation of eIF2α attenuates global translation (Holcik 2015), however the selective translation of mRNAs harbouring IRESs and uORFs—both of which have been shown to be regulated by eIF5B- is activated (Fitzgerald and Semler 2009; Thakor and Holcik 2012). We previously showed that eIF5B plays a role in uORF-mediated translational regulation of master transcription factor ATF4 (Ross et al. 2018). ATF4 has been implicated in

regulating the cellular transcriptome in multiple cell lines; specifically, in the presence of mitochondrial stress, ATF4 has been shown to coordinate cytoprotective genes and the cellular metabolism (Quiros et al. 2017). In addition, RNA-sequencing of mice with a liver-specific ATF4 deletion revealed that many genes require ATF4 for full expression during basal conditions (Fusakio et al. 2016). Moreover, ATF4 is required for the expression of 7.5% of genes regulated by ER stress, including those involved in amino acid metabolism and cholesterol metabolism (Fusakio et al. 2016). Assessing both ATF4-depleted and ATF4-overexpressing hippocampal neurons showed Sestrin 2 (Sesn2) as a positive regulatory target, which protects cells from oxidative and genotoxic stress from reactive oxygen species (ROS) and inhibits mTORC1 (Liu et al. 2018). These studies highlight the transcriptome-wide consequences of dysregulation of just one transcription factor.

Interestingly, we have previously demonstrated that eIF5B represses the translation of *ATF4* in HEK 293T cells, with minimal effects on the steady state mRNA levels of *ATF4* (Ross et al. 2018). The present study corroborates those findings, with transcriptome analysis showing no significant difference in *ATF4* transcript levels in eIF5B-depleted cells (Supplemental Figure 1). We have previously characterized GADD34 to be upregulated at both the RNA and protein level upon eIF5B-depletion (Ross et al. 2018). Here we additionally show that the transcript levels of *GADD34* (PPP1R15A) are significantly upregulated upon eIF5B depletion (Supplemental Figure 1). *GADD34* is a direct target of ATF4 that acts as a negative feedback loop in the ISR by dephosphorylating eIF2α (Carroll et al. 2006). Our transcriptome data further shows *CHOP* to be upregulated upon eIF5B depletion (Supplemental Figure 1). CHOP is another transcription factor involved in the ISR that forms dimers with ATF4 when stress is prolonged, pushing cells towards apoptosis (Su and Kilberg 2008). It has been shown that the overexpression of CHOP promotes apoptosis, while cells deficient in CHOP become resistant to ER stress-induced apoptosis (Kim et al. 2008; Oyadomari and Mori 2004). Depletion of eIF5B removes the repression of *ATF4* translation and as a result, the transcription of *CHOP* and *GADD34* is enhanced.

We have observed that eIF5B-depleted cells expressed higher levels of CHOP and GADD34 (Figure 3 and Supplemental Figure S2), likely due to enhanced translation of *ATF4* mRNA leading to enhanced ATF4 protein level. Surprisingly, BiP levels were significantly reduced in eIF5B-depleted HEK 293T cells (Figure 3 and Supplemental Figure S2). Interestingly, BiP expression is

regulated at the mRNA translation level via IRES element (Cho et al. 2007). It is possible that eIF5B regulates the IRES-mediated translation of BiP and thereby depletion of eIF5B may have resulted in the decreased levels of BiP. Enhanced CHOP levels and decreased BiP levels have been shown to activate lysosomal degradation of heat sock protein factor 1 (HSF1) (Kim et al. 2017). In fact, we have also observed enhanced levels of CHOP and decreased levels of BiP in eIF5B-depleted cells concurrent with modestly decreased levels of HSF1 (Figure 3 and Supplemental Figure S2). We have also observed decreased levels of phosphorylated HSF1 protein despite phosphorylation of JNK (Figure 3 and Supplemental Figure S2). Furthermore, the levels of XBP1 mRNA was enhanced in eIF5B-depleted cells (Supplemental Table 2). We also show that XBP1 proteins levels are also enhanced in eIF5B-depleted cells. This could have been due to the decrease levels of BiP in these cells. Decreased expression on BiP would derepress inositol requiring enzyme 1 (IRE1) and would in turn enhance the expression of XBP1. Enhanced XBP1 expression is clearly linked to ER stress (van Schadewijk et al. 2012). This validates the changes we observed in transcriptome profile affected by the levels of eIF5B. As ER stress is known to activate apoptosis (Lumley et al. 2017), collectively, these findings suggest that eIF5B depletion activates the pro-apoptotic ER stress in HEK 293T cells.

Interestingly, transcriptional misregulation in cancer was significantly affected by the depletion of eIF5B (Table 2, Supplemental Figure 1). Several key transcription factors of *E26 transformation-specific (ETS) variant transcription factor 1 (ETV1)*, *ETV5*, and *homeobox A10 (HOXA10)* were downregulated upon eIF5B depletion (Supplemental Figure 1). HOX family proteins are frequently deregulated in cancer, and they encode transcription factors involved in cell growth and identity, as well as cell-cell and cell-extracellular matrix interactions (Abate-Shen 2002; Carrera et al. 2015). In head and neck squamous cell carcinoma (HNSCC), 18 HOX genes including *HOXA10* had higher expression levels in pre-malignant and cancerous tissue as compared to normal tissue (Darda et al. 2015). However the role of HOX proteins is not fully understood. HOXA10 overexpression promotes the progression of endometrial cancer (Guo et al. 2018; Yoshida et al. 2006), yet the inhibition of HOXA10 is associated with breast cancer tumorigenesis (Chu et al. 2004). Though the mechanism is not fully understood, it has been shown that HOXA10 can mediate signaling through p53 and p21 activation, as well as cKit and signal transducer and activator of transcription 3 (STAT3) repression to inhibit testicular cell proliferation (Chen et al. 2018). HOXA10 has been shown to increase

temozolomide resistance in glioblastoma, (Kim et al. 2014) and to regulate G1 phase arrest (Zhang et al. 2014), showing its critical role in cell proliferation and division. In addition to HOX proteins, ETS proteins are also highly correlated to cancer progression. The ETS family transcription factors have a PEA3 subgroup (ETV1, ETV4, ETV5) that are activated by Ras/ MAPK signaling (Laudet et al. 1999). Overexpression of ETV1 and ETV4 is linked to prostate cancer (Tomlins et al. 2007; Vitari et al. 2011), and drives an oncogenic program in gastrointestinal stromal tumors (Chi et al. 2010). The downregulation of HOXA10, ETV1, and ETV5 upon eIF5B depletion, further supports the role of eIF5B in critical signaling pathways through its regulation of master transcription factors.

T-cell receptor signaling was shown to be downregulated upon eIF5B depletion (Table 2, Supplemental Figure 1), including specific target interleukin-1 receptor (IL1R). IL-1 is a master regulator of inflammation controlling innate immune responses (Dinarello 2009). Two members of the IL-1 family: IL-1α and IL-1β, are cytokines that both signal through IL1R (Dinarello 2009; Gabay et al. 2010). In the tumor microenvironment, tumor-associated macrophages, glioblastoma cells themselves, and non-enoplastic brain cells are able to produce active IL-1β (Kennedy et al. 2013; Stanimirovic et al. 2001; Yamanaka et al. 1994). IL-1β activation has been shown to promote hypoxia-induced death in glioblastoma through inhibition of hypoxia-inducible factor 1 (HIF1) activity (Sun et al. 2014). Dexamethasone which treats development of glioblastoma-associated cerebral oedema, inhibits the production of IL-1 cytokines, suggesting IL-1 inhibition as a therapeutic (Herting et al. 2019). It has been suggested that the IL-1 induced tumor secretome, can modulate the glioma and tumor microenvironment including tumor cell survival, invasion, tumor angiogenesis, and anti-tumor immunity (Tarassishin et al. 2014).

Mucin-type O-glycan biosynthesis was shown to be upregulated upon eIF5B depletion (Table 1, Supplemental Figure 1). Mucin-type O-glycosylation is the initial addition of a N-acetylgalactosamine (GalNAc) sugar to the hydroxyl group of serine or threonine residues. Mucin-type O-glycans are found on many cell surface and secreted proteins, and function to coordinate recognition, adhesion, and communication between cells (Tran and Ten Hagen 2013). Mucin-type O-glycosylation is controlled by a family of approximately 20 homologous genes encoding UDP-GalNac:polypeptide Gal NAc transferases (GALNTs) (Guzman-Aranguez and Argueso 2010). GALNTs are differentially expressed in malignant tissue as compared to normal tissue, suggesting a

role for O-glycosylation in cancer. GALNT3 promotes the growth of pancreatic cancer cells, while mutations in GALNT12 that encode a nonfunctional enzyme are associated with colon cancer development (Guda et al. 2009; Taniuchi et al. 2011). An assessment of 14 GALNTs found that GALNT9 gene expression was correlated to better clinical outcome in neuroblastoma patients (Berois et al. 2013). Genetic ablation of various GALNTs in mice has caused defective angiogenesis, fatal brain hemorrhages, and additional consequences (An et al. 2007; Stone et al. 2009; Xia et al. 2004). Though the full mechanisms of GALNTs and O-glycosylation is not fully understood in cancer, our data that eIF5B effects mucin-type O-glycan biosynthesis, suggests a further role for eIF5B in critical cell processes.

Our transcriptome data suggests that certain genes involved in MAPK signaling are differentially expressed in eIF5B-depleted cells (Table 3), and we confirmed an increase in phosphorylation of JNK in eIF5B depleted cells (Figure 3 and Supplemental Figure S2). Furthermore, we also observed that certain target genes of JNK/c-Jun/AP-1 are differentially expressed in eIF5B-depleted cells (Table 3). A recent study determined select proteins, including beta-arrestin-1 (ARRB1), isoform tau-A or tau, APK-activated protein kinase 2 (MAPKAPK2), S6 kinase alpha-3 (RPS6KA3), MAPK1, MAPK3, MAPK12, and MAPK14 to be downregulated significantly upon eIF5B depletion (Jiang et al. 2016). We did not observe significant up- or down-regulation for the transcripts corresponding to those proteins, but we did observe upregulation of select transcripts involved in MAPK signaling (Table 3). Notably, in contrast to our transient knockdown of eIF5B—which reproducibly achieved approximately ~90% eIF5B silencing—the study by Jiang et al. (2016) used the CRISPR/Cas9 method to maintain an approximately 50% knockdown. We suggest that the significant difference in eIF5B levels between the two studies contributed to the deviation in observed pathways affected, including MAPK. Additionally, our transient transfection is more likely to reflect short-term and direct changes of eIF5B-depletion, while Jiang et al. (2016) used chronic, long-term eIF5B depletion, which could reveal more indirect consequences. Jiang et al. (2016) observed that ~50% eIF5B depletion results in both decreased ROS and a prolonged S-phase. These opposing observations suggest that the variation in knockdown efficiency and/or methodology between Jiang et al. (2016) and the present study is important and results in significantly different physiological outcomes. Based

on these observations, we conclude that eIF5B depletion results in activation of at least the JNK-arm of the MAPK pathway.

For the first time we have implicated eIF5B in the pro-apoptotic ER stress and also demonstrated that although eIF5B is a translation initiation factor, it has an indirect role in regulating the transcriptome of the cell. Our finding that eIF5B depletion results in upregulated MAPK signaling—specifically, JNK-phosphorylation—suggests that eIF5B may influence many cellular pathways, including proliferation, apoptosis, and the cell cycle. eIF5B might thus represent an important regulatory hub, potentially offering novel insights into cellular biology in health and disease.

Author Contributions: Conceptualization, K.R.B., and N.T.; Transcriptome Data Analysis, S.I., K.V.D. and A.Z. ; Investigation, K.R.B., J.A.R., K.V.D., K.T., and K.P. ; Resources, N.T., I.K. and A.Z.; Writing and Editing, K.R.B., J.A.R., N.T.; Funding Acquisition, N.T.

Acknowledgements: K.R.B was supported by NSERC-CGS and Queen Elizabeth II fellowships. K.V.D. was supported by Queen Elizabeth II and Alberta Innovates Tech Future graduate fellowships. K.P. and J.A.R, undergraduate and postdoctoral fellow respectively, were partially supported by NSERC-CREATE grant (510937-2018). This work was funded by a Natural Sciences and Engineering Research Council of Canada-Discovery Grant (RGPIN-2017-05463), the Canada Foundation for Innovation-John R. Evans Leaders Fund (35017), the Campus Alberta Innovates Program and the Alberta Ministry of Economic Development and Trade.

Conflicts of Interest: The authors declare no competing interests.

References

Abate-Shen C (2002) Deregulated homeobox gene expression in cancer: cause or consequence? Nat Rev Cancer 2:777-785 doi:10.1038/nrc907

An G et al. (2007) Increased susceptibility to colitis and colorectal tumors in mice lacking core 3-derived O-glycans J Exp Med 204:1417-1429 doi:10.1084/jem.20061929

Berois N et al. (2013) GALNT9 gene expression is a prognostic marker in neuroblastoma patients Clin Chem 59:225-233 doi:10.1373/clinchem.2012.192328

Calvo SE, Pagliarini DJ, Mootha VK (2009) Upstream open reading frames cause widespread reduction of protein expression and are polymorphic among humans Proceedings of the National Academy of Sciences 106:7507-7512 doi:10.1073/pnas.0810916106

Carrera M et al. (2015) HOXA10 controls proliferation, migration and invasion in oral squamous cell carcinoma Int J Clin Exp Pathol 8:3613-3623

Carroll M, Dyer J, Sossin WS (2006) Serotonin increases phosphorylation of synaptic 4EBP through TOR, but eukaryotic initiation factor 4E levels do not limit somatic cap-dependent translation in aplysia neurons Mol Cell Biol 26:8586-8598 doi:10.1128/MCB.00955-06

Chen R, Li H, Li Y, Fazli L, Gleave M, Nappi L, Dong X (2018) Loss of Nuclear Functions of HOXA10 Is Associated With Testicular Cancer Proliferation Front Oncol 8:594 doi:10.3389/fonc.2018.00594

Chi P et al. (2010) ETV1 is a lineage survival factor that cooperates with KIT in gastrointestinal stromal tumours Nature 467:849-853 doi:10.1038/nature09409

Cho S, Park SM, Kim TD, Kim JH, Kim KT, Jang SK (2007) BiP internal ribosomal entry site activity is controlled by heat-induced interaction of NSAP1 Mol Cell Biol 27:368-383 doi:10.1128/MCB.00814-06

Chu MC, Selam FB, Taylor HS (2004) HOXA10 regulates p53 expression and matrigel invasion in human breast cancer cells Cancer Biol Ther 3:568-572 doi:10.4161/cbt.3.6.848

Czeh G, Czopf J (1991) An intracellular investigation into the postsynaptic responses of the principal cells in slice preparations from rat hippocampal formation Acta Physiol Hung 77:63-76

Darda L, Hakami F, Morgan R, Murdoch C, Lambert DW, Hunter KD (2015) The role of HOXB9 and miR-196a in head and neck squamous cell carcinoma PLoS One 10:e0122285 doi:10.1371/journal.pone.0122285

Darling NJ, Cook SJ (2014) The role of MAPK signalling pathways in the response to endoplasmic reticulum stress Biochim Biophys Acta 1843:2150-2163 doi:10.1016/j.bbamcr.2014.01.009

Dey S, Baird TD, Zhou D, Palam LR, Spandau DF, Wek RC (2010) Both transcriptional regulation and translational control of ATF4 are central to the integrated stress response J Biol Chem 285:33165-33174 doi:10.1074/jbc.M110.167213

Dinarello CA (2009) Immunological and inflammatory functions of the interleukin-1 family Annu Rev Immunol 27:519-550 doi:10.1146/annurev.immunol.021908.132612

Faye MD, Graber TE, Holcik M (2014) Assessment of selective mRNA translation in mammalian cells by polysome profiling J Vis Exp:e52295 doi:10.3791/52295

Fitzgerald KD, Semler BL (2009) Bridging IRES elements in mRNAs to the eukaryotic translation apparatus Biochim Biophys Acta 1789:518-528 doi:10.1016/j.bbagrm.2009.07.004

Fusakio ME et al. (2016) Transcription factor ATF4 directs basal and stress-induced gene expression in the unfolded protein response and cholesterol metabolism in the liver Mol Biol Cell 27:1536-1551 doi:10.1091/mbc.E16-01-0039

Gabay C, Lamacchia C, Palmer G (2010) IL-1 pathways in inflammation and human diseases Nat Rev Rheumatol 6:232-241 doi:10.1038/nrrheum.2010.4

Graber TE, Holcik M (2007) Cap-independent regulation of gene expression in apoptosis Mol Biosyst 3:825-834 doi:10.1039/b708867a

Guda K et al. (2009) Inactivating germ-line and somatic mutations in polypeptide N-acetylgalactosaminyltransferase 12 in human colon cancers Proc Natl Acad Sci U S A 106:12921-12925 doi:10.1073/pnas.0901454106

Guo LM, Ding GF, Xu W, Ge H, Jiang Y, Chen XJ, Lu Y (2018) MiR-135a-5p represses proliferation of HNSCC by targeting HOXA10 Cancer Biol Ther 19:973-983 doi:10.1080/15384047.2018.1450112

Guzman-Aranguez A, Argueso P (2010) Structure and biological roles of mucin-type O-glycans at the ocular surface Ocul Surf 8:8-17 doi:10.1016/s1542-0124(12)70213-6

Herting CJ, Chen Z, Maximov V, Duffy A, Szulzewsky F, Shayakhmetov DM, Hambardzumyan D (2019) Tumour-associated macrophage-derived interleukin-1 mediates glioblastoma-associated cerebral oedema Brain 142:3834-3851 doi:10.1093/brain/awz331

Ho JJD, Balukoff NC, Cervantes G, Malcolm PD, Krieger JR, Lee S (2018) Oxygen-Sensitive Remodeling of Central Carbon Metabolism by Archaic eIF5B Cell Reports 22:17-26 doi:10.1016/j.celrep.2017.12.031

Holcik M (2015) Could the eIF2α-Independent Translation Be the Achilles Heel of Cancer? Frontiers in oncology 5:264 doi:10.3389/fonc.2015.00264

Holcik M, Sonenberg N (2005) Translational control in stress and apoptosis Nat Rev Mol Cell Biol 6:318-327 doi:10.1038/nrm1618

Huang da W, Sherman BT, Lempicki RA (2009a) Bioinformatics enrichment tools: paths toward the comprehensive functional analysis of large gene lists Nucleic Acids Res 37:1-13 doi:10.1093/nar/gkn923

Huang da W, Sherman BT, Lempicki RA (2009b) Systematic and integrative analysis of large gene lists using DAVID bioinformatics resources Nat Protoc 4:44-57 doi:10.1038/nprot.2008.211

Jiang X, Jiang X, Feng Y, Xu R, Wang Q, Deng H (2016) Proteomic Analysis of eIF5B Silencing-Modulated Proteostasis PLoS One 11:e0168387 doi:10.1371/journal.pone.0168387

Kanehisa M, Goto S (2000) KEGG: kyoto encyclopedia of genes and genomes Nucleic Acids Res 28:27-30 doi:10.1093/nar/28.1.27

Kennedy BC, Showers CR, Anderson DE, Anderson L, Canoll P, Bruce JN, Anderson RC (2013) Tumor-associated macrophages in glioma: friend or foe? J Oncol 2013:486912 doi:10.1155/2013/486912

Kim D, Langmead B, Salzberg SL (2015) HISAT: a fast spliced aligner with low memory requirements Nat Methods 12:357-360 doi:10.1038/nmeth.3317

Kim E, Sakata K, Liao FF (2017) Bidirectional interplay of HSF1 degradation and UPR activation promotes tau hyperphosphorylation PLoS Genet 13:e1006849 doi:10.1371/journal.pgen.1006849

Kim I, Xu W, Reed JC (2008) Cell death and endoplasmic reticulum stress: disease relevance and therapeutic opportunities Nat Rev Drug Discov 7:1013-1030 doi:10.1038/nrd2755

Kim JW, Kim JY, Kim JE, Kim SK, Chung HT, Park CK (2014) HOXA10 is associated with temozolomide resistance through regulation of the homologous recombinant DNA repair pathway in glioblastoma cell lines Genes Cancer 5:165-174 doi:10.18632/genesandcancer.16

Laudet V, Hanni C, Stehelin D, Duterque-Coquillaud M (1999) Molecular phylogeny of the ETS gene family Oncogene 18:1351-1359 doi:10.1038/sj.onc.1202444

Lee S, Truesdell SS, Bukhari SI, Lee JH, LeTonqueze O, Vasudevan S (2014) Upregulation of eIF5B controls cell-cycle arrest and specific developmental stages Proc Natl Acad Sci U S A 111:E4315-4322 doi:10.1073/pnas.1320477111

Liao Y, Smyth GK, Shi W (2014) featureCounts: an efficient general purpose program for assigning sequence reads to genomic features Bioinformatics 30:923-930 doi:10.1093/bioinformatics/btt656

Liu J et al. (2018) Brain-Derived Neurotrophic Factor Elevates Activating Transcription Factor 4 (ATF4) in Neurons and Promotes ATF4-Dependent Induction of Sesn2 Front Mol Neurosci 11:62 doi:10.3389/fnmol.2018.00062

Love MI, Huber W, Anders S (2014) Moderated estimation of fold change and dispersion for RNA-seq data with DESeq2 Genome Biol 15:550 doi:10.1186/s13059-014-0550-8

Lumley EC et al. (2017) Moderate endoplasmic reticulum stress activates a PERK and p38-dependent apoptosis Cell Stress Chaperones 22:43-54 doi:10.1007/s12192-016-0740-2

Oyadomari S, Mori M (2004) Roles of CHOP/GADD153 in endoplasmic reticulum stress Cell Death Differ 11:381-389 doi:10.1038/sj.cdd.4401373

Pakos-Zebrucka K, Koryga I, Mnich K, Ljujic M, Samali A, Gorman AM (2016) The integrated stress response EMBO Rep 17:1374-1395 doi:10.15252/embr.201642195

Pestova TV, de Breyne S, Pisarev AV, Abaeva IS, Hellen CU (2008) eIF2-dependent and eIF2-independent modes of initiation on the CSFV IRES: a common role of domain II EMBO J 27:1060-1072 doi:10.1038/emboj.2008.49

Quiros PM et al. (2017) Multi-omics analysis identifies ATF4 as a key regulator of the mitochondrial stress response in mammals J Cell Biol 216:2027-2045 doi:10.1083/jcb.201702058

Raciti M, Lotti LV, Valia S, Pulcinelli FM, Di Renzo L (2012) JNK2 is activated during ER stress and promotes cell survival Cell Death Dis 3:e429 doi:10.1038/cddis.2012.167

Ross JA, Bressler KR, Thakor N (2018) Eukaryotic Initiation Factor 5B (eIF5B) Cooperates with eIF1A and eIF5 to Facilitate uORF2-Mediated Repression of ATF4 Translation Int J Mol Sci 19 doi:10.3390/ijms19124032

Ross JA, Dungen KV, Bressler KR, Fredriksen M, Khandige Sharma D, Balasingam N, Thakor N (2019) Eukaryotic initiation factor 5B (eIF5B) provides a critical cell survival switch to glioblastoma cells via regulation of apoptosis Cell Death Dis 10:57 doi:10.1038/s41419-018-1283-5

Sharma DK, Bressler K, Patel H, Balasingam N, Thakor N (2016) Role of Eukaryotic Initiation Factors during Cellular Stress and Cancer Progression Journal of Nucleic Acids 2016:8235121-8235119 doi:10.1155/2016/8235121

Stanimirovic D, Zhang W, Howlett C, Lemieux P, Smith C (2001) Inflammatory gene transcription in human astrocytes exposed to hypoxia: roles of the nuclear factor-kappaB and autocrine stimulation J Neuroimmunol 119:365-376 doi:10.1016/s0165-5728(01)00402-7

Starck SR et al. (2016) Translation from the 5' untranslated region shapes the integrated stress response Science 351:aad3867 doi:10.1126/science.aad3867

Stone EL et al. (2009) Glycosyltransferase function in core 2-type protein O glycosylation Mol Cell Biol 29:3770-3782 doi:10.1128/MCB.00204-09

Su N, Kilberg MS (2008) C/EBP homology protein (CHOP) interacts with activating transcription factor 4 (ATF4) and negatively regulates the stress-dependent induction of the asparagine synthetase gene J Biol Chem 283:35106-35117 doi:10.1074/jbc.M806874200

Sun W, Depping R, Jelkmann W (2014) Interleukin-1beta promotes hypoxia-induced apoptosis of glioblastoma cells by inhibiting hypoxia-inducible factor-1 mediated adrenomedullin production Cell Death Dis 5:e1020 doi:10.1038/cddis.2013.562

Taniuchi K et al. (2011) Overexpression of GalNAc-transferase GalNAc-T3 promotes pancreatic cancer cell growth Oncogene 30:4843-4854 doi:10.1038/onc.2011.194

Tarassishin L, Lim J, Weatherly DB, Angeletti RH, Lee SC (2014) Interleukin-1-induced changes in the glioblastoma secretome suggest its role in tumor progression J Proteomics 99:152-168 doi:10.1016/j.jprot.2014.01.024

Terenin IM, Dmitriev SE, Andreev DE, Shatsky IN (2008) Eukaryotic translation initiation machinery can operate in a bacterial-like mode without eIF2 Nat Struct Mol Biol 15:836-841 doi:10.1038/nsmb.1445

Thakor N, Holcik M (2012) IRES-mediated translation of cellular messenger RNA operates in eIF2α-independent manner during stress Nucleic Acids Research 40:541-552 doi:10.1093/nar/gkr701

Tomlins SA et al. (2007) Distinct classes of chromosomal rearrangements create oncogenic ETS gene fusions in prostate cancer Nature 448:595-599 doi:10.1038/nature06024

Tran DT, Ten Hagen KG (2013) Mucin-type O-glycosylation during development J Biol Chem 288:6921-6929 doi:10.1074/jbc.R112.418558

van Schadewijk A, van't Wout EF, Stolk J, Hiemstra PS (2012) A quantitative method for detection of spliced X-box binding protein-1 (XBP1) mRNA as a measure of endoplasmic reticulum (ER) stress Cell Stress Chaperones 17:275-279 doi:10.1007/s12192-011-0306-2

Vitari AC et al. (2011) COP1 is a tumour suppressor that causes degradation of ETS transcription factors Nature 474:403-406 doi:10.1038/nature10005

Xia L et al. (2004) Defective angiogenesis and fatal embryonic hemorrhage in mice lacking core 1-derived O-glycans J Cell Biol 164:451-459 doi:10.1083/jcb.200311112

Yamanaka R, Tanaka R, Saitoh T, Okoshi S (1994) Cytokine gene expression on glioma cell lines and specimens J Neurooncol 21:243-247 doi:10.1007/bf01063773

Yoshida H, Broaddus R, Cheng W, Xie S, Naora H (2006) Deregulation of the HOXA10 homeobox gene in endometrial carcinoma: role in epithelial-mesenchymal transition Cancer Res 66:889-897 doi:10.1158/0008-5472.CAN-05-2828

Zhang L et al. (2014) Upregulation HOXA10 homeobox gene in endometrial cancer: role in cell cycle regulation Med Oncol 31:52 doi:10.1007/s12032-014-0052-2

Tables:

Table 1

Name		Log2 Fold Change	ENSEMBL GENE ID	Species
has:00512 Mucin type O-Glycan biosynthesis				
ST3GAL1	ST3 beta-galactoside alpha-2,3-sialyltransferase 1	1.647635	ENSG00000008513	*Homo sapiens*
GALNT8	polypeptide N-acetylgalactosaminyltransferase 8	2.653729	ENSG00000130035	*Homo sapiens*
GALNT14	polypeptide N-acetylgalactosaminyltransferase 14	2.055928	ENSG00000158089	*Homo sapiens*
has:04080 Neuroactive ligand-receptor interaction				
GRIK3	glutamate ionotropic receptor kainate type subunit 3	4.990015989	ENSG00000163873	*Homo sapiens*
P2RX1	purinergic receptor P2X 1	4.798947295	ENSG00000108405	*Homo sapiens*
GRM4	glutamate metabotropic receptor 4	5.646421068	ENSG00000124493	*Homo sapiens*
CHRNB2	cholinergic receptor nicotinic beta 2 subunit	5.171089524	ENSG00000160716	*Homo sapiens*
DRD2	dopamine receptor D2	3.88159386	ENSG00000149295	*Homo sapiens*
HRH3	histamine receptor H3	4.963651756	ENSG00000101180	*Homo sapiens*
CHRNA4	cholinergic receptor nicotinic alpha 4 subunit	2.219764154	ENSG00000101204	*Homo sapiens*
GABBR2	gamma-aminobutyric acid type B receptor subunit 2	2.512753405	ENSG00000136928	*Homo sapiens*
GRIK3	glutamate ionotropic receptor kainate type subunit 3	4.990015989	ENSG00000163873	*Homo sapiens*
has:04141 Protein processing in endoplasmic reticulum				
GANAB	glucosidase II alpha subunit	2.414058365	ENSG00000089597	*Homo sapiens*
PARK2	parkin RBR E3 ubiquitin protein ligase	3.399428902	ENSG00000185345	*Homo sapiens*
PPP1R15A	protein phosphatase 1 regulatory subunit 15A	2.604650462	ENSG00000087074	*Homo sapiens*
XBP1	X-box binding protein 1	1.74970712	ENSG00000100219	*Homo sapiens*
DDIT3	DNA damage inducible transcript 3	3.042748774	ENSG00000175197	*Homo sapiens*
HYOU1	hypoxia up-regulated 1	1.685701269	ENSG00000149428	*Homo sapiens*
RAD23A	RAD23 homolog A, nucleotide excision repair protein	2.055191193	ENSG00000179262	*Homo sapiens*
has:04721 Synaptic vesicle cycle				
UNC13A	unc-13 homolog A	2.034621777	ENSG00000130477	*Homo sapiens*
CPLX1	complexin 1	2.926850953	ENSG00000168993	*Homo sapiens*
CPLX2	complexin 2	6.546761306	ENSG00000145920	*Homo sapiens*
ATP6V0D2	ATPase H+ transporting V0 subunit d2	2.583641031	ENSG00000147614	*Homo sapiens*

Table 1. Significantly up-regulated genes upon eIF5B depletion in HEK 293T cells. Transcriptome analysis was performed on 3 biological replicates and the data were sorted *via* GOstats pathway analysis.

Table 2

Name		Log2 Fold Change	ENSEMBL GENE ID	Species
has:05202 Transcriptional Misregulation in Cancer				
ETV5	ETS variant 5	-2.154098145	ENSG00000244405	*Homo sapiens*
MAF	MAF bZIP transcription factor	-1.44832678	ENSG00000178573	*Homo sapiens*
CDKN2C	cyclin dependent kinase inhibitor 2C	-1.301358154	ENSG00000123080	*Homo sapiens*
ETV1	ETS variant 1	-2.727531685	ENSG00000006468	*Homo sapiens*
HOXA10	homeobox A10	-1.763867776	ENSG00000253293	*Homo sapiens*
has:05166 HTLV-I Infection				
EGR1	early growth response 1	-2.14323631	ENSG00000120738	*Homo sapiens*
TP53INP1	tumor protein p53 inducible nuclear protein 1	-2.365233867	ENSG00000164938	*Homo sapiens*
HLA-DMB	major histocompatibility complex, class II, DM beta	-1.906033177	ENSG00000242574	*Homo sapiens*
CDKN2C	cyclin dependent kinase inhibitor 2C	-1.301358154	ENSG00000123080	*Homo sapiens*
IL1R1	interleukin 1 receptor type 1	-2.600867502	ENSG00000115594	*Homo sapiens*

Table 2. Significantly down-regulated genes upon eIF5B depletion in HEK 293T cells. Transcriptome analysis was performed on 3 biological replicates and the data were sorted *via* GOstats pathway analysis.

Table 3

Examples of Genes involved in MAPK				
Name		**Log2 Fold Change**	**ENSEMBL Gene ID**	**Species**
DDIT3	DNA damage inducible transcript 3	3.042749	ENSG00000175197	*Homo sapiens*
FGFR4	Fibroblast growth factor receptor 4	2.313778	ENSG00000160867	*Homo sapiens*
PDGFA	Platelet derived growth factor subunit A	2.056486	ENSG00000197461	*Homo sapiens*
RASGRF2	Ras protein specific guanine nucleotide releasing factor 2	1.739305	ENSG00000113319	*Homo sapiens*
FGF21	Fibroblast growth factor 21	4.092756	ENSG00000105550	*Homo sapiens*
MAPK15	Mitogen-activated protein kinase 15	2.231672	ENSG00000181085	*Homo sapiens*
MAP2K6	Mitogen-activated protein kinase 6	-2.54435	ENSG00000108984	*Homo sapiens*
VGF	VGF nerve growth factor inducible	2.564835	ENSG00000128564	*Homo sapiens*
Examples of Genes involved in JNK/C-Jun/AP-1 axis				
BATF3	Basic leucine zipper ATF-like transcription factor 3	2.306892	ENSG00000123685	*Homo sapiens*
CD9	CD9 molecule	-2.5409	ENSG00000010278	*Homo sapiens*
DKK3	Dickkopf WNT signaling pathway inhibitor 3	-1.66459	ENSG00000050165	*Homo sapiens*
AUP1	AUP1	2.280739	ENSG00000115307	*Homo sapiens*

Table 3. Differentially express genes that are involved in MAPK and JNK pathways in eIF5B-depleted cells.

Figure legends

Figure 1. (A) Normalized expression of eIF5B in control (C) and eIF5B-depleted (5B) HEK 293T samples; numbers (1, 2 and 3) indicate independent biological replicates. **(B)** Volcano plot confirming significantly upregulated (right) and downregulated (left) transcripts, where blue denotes a significant change ($p < 0.05$). **(C)** Heatmap showing the differentially-expressed genes upon eIF5B depletion. Red and green indicate up-regulation and down-regulation, respectively, upon eIF5B depletion.

Figure 2. Validation of RNA-seq results. Total RNA was purified from an independent set of control and eIF5B-depleted cells and subjected to RT-qPCR. Steady-state levels of the transcripts expected—based on the transcriptome profile—to be most up-regulated **(A)** or down-regulated **(B)** upon eIF5B depletion were quantified. Data represent the mean ± SEM for 3 independent biological replicates. *, $p < 0.05$; **, $p < 0.01$; ***, $p < 0.001$; ****, $p < 0.0001$.

Figure 3. Depletion of eIF5B leads to activation of ER stress and increased levels of the phosphorylated JNK protein in HEK 293T cells. HEK 293T cells were transfected with a non-specific control siRNA (siC) or an eIF5B-specific siRNA pool (si5B) and resolved by SDS-PAGE before performing immunoblotting. **(A)** Representative immunoblots probing for eIF5B, total JNK (P54 and P46), phospho-JNK (P54 and P46), HSF1, phosphor-HSF1, BIP, CHOP, GADD34, XBP1 and β-actin (internal control). **(B-K)** Quantitation of these proteins, all normalized to β-actin. Data are expressed as mean ± SEM for 3 independent biological replicates. **, $p < 0.01$; ****, $p < 0.0001$.

A

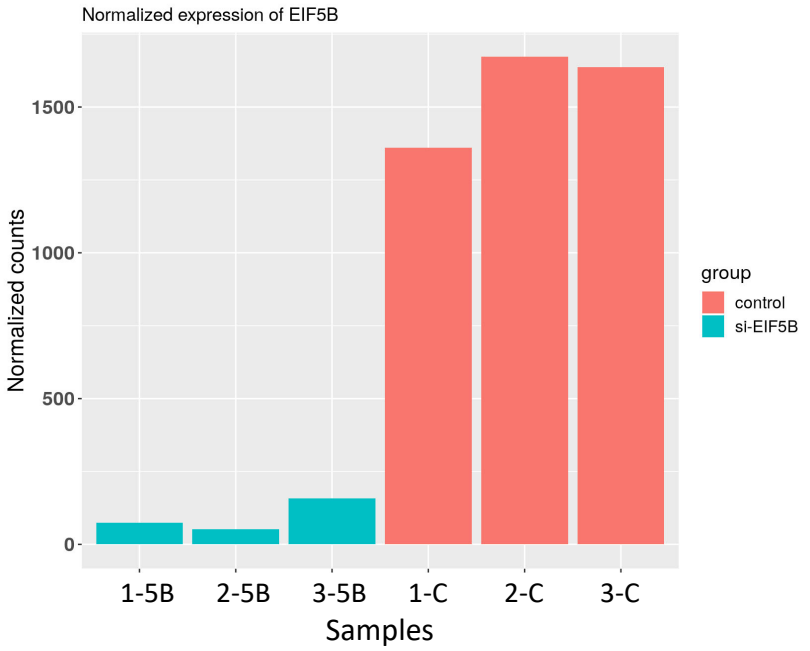
Normalized expression of EIF5B
Normalized counts
1500
1000
500
0
1-5B
2-5B
3-5B
1-C
2-C
3-C
Samples
group
control
si-EIF5B

B

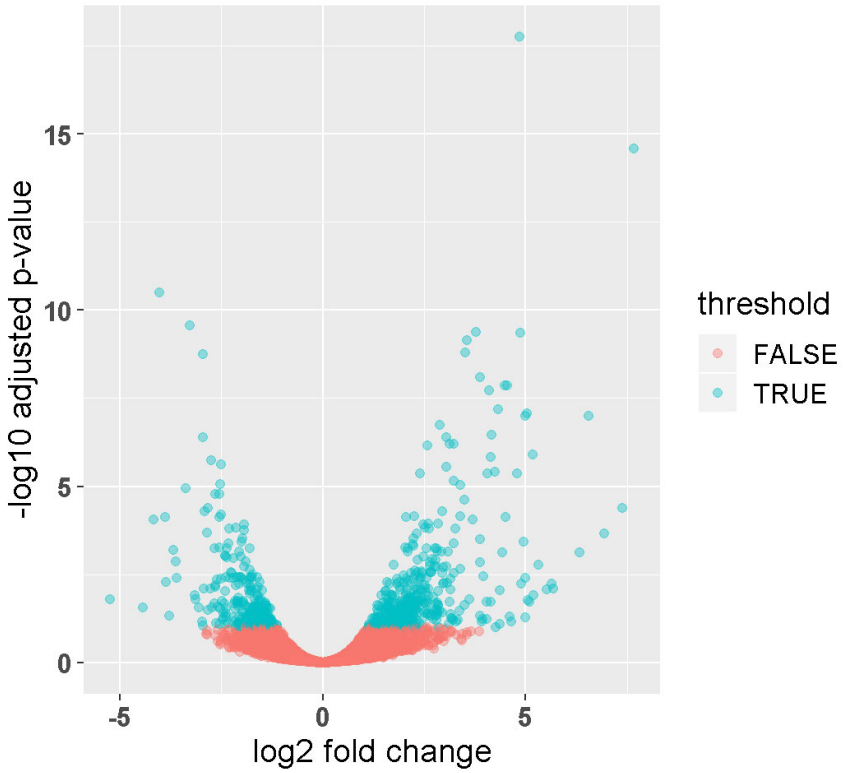
-log10 adjusted p-value
15
10
5
0
-5
0
5
log2 fold change
threshold
FALSE
TRUE

C

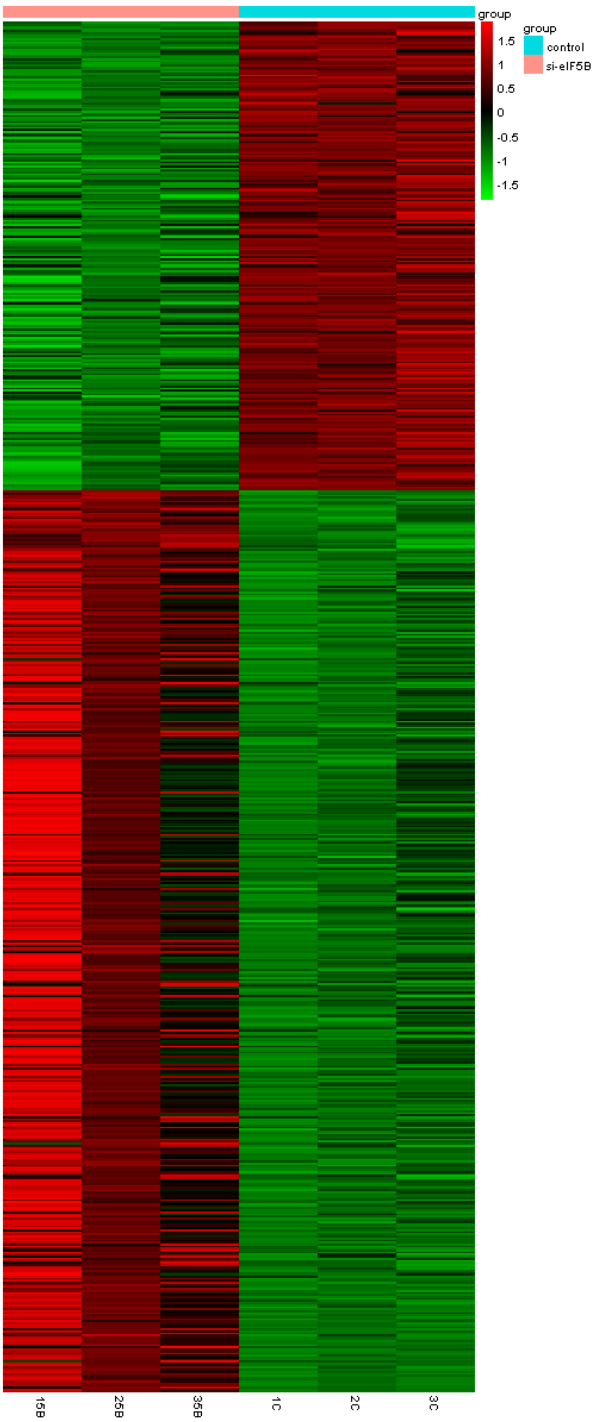
group
1.5
1
0.5
0
-0.5
-1
-1.5
group
control
si-eIF5B
1B
2B
3B
1C
2C
3C

A

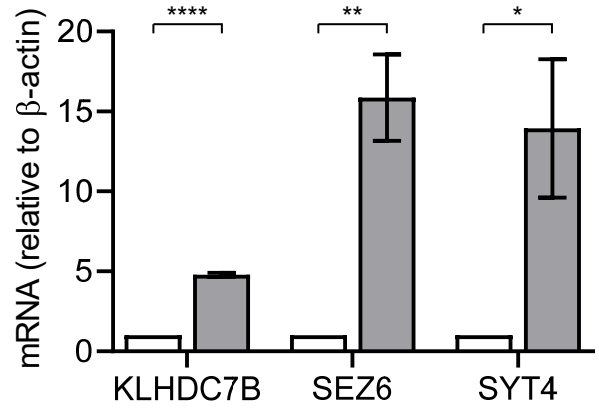
****
**
*
20
15
10
5
0
mRNA (relative to β-actin)
KLHDC7B
SEZ6
SYT4

B

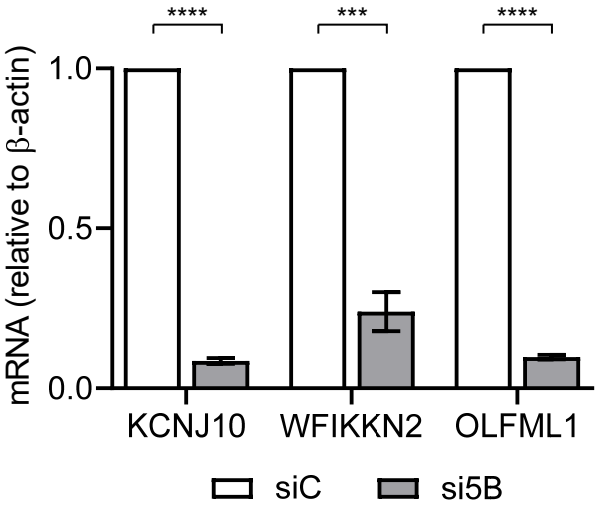
****
***
****
1.0
0.5
0.0
mRNA (relative to β-actin)
KCNJ10
WFIKKN2
OLFML1
siC
si5B

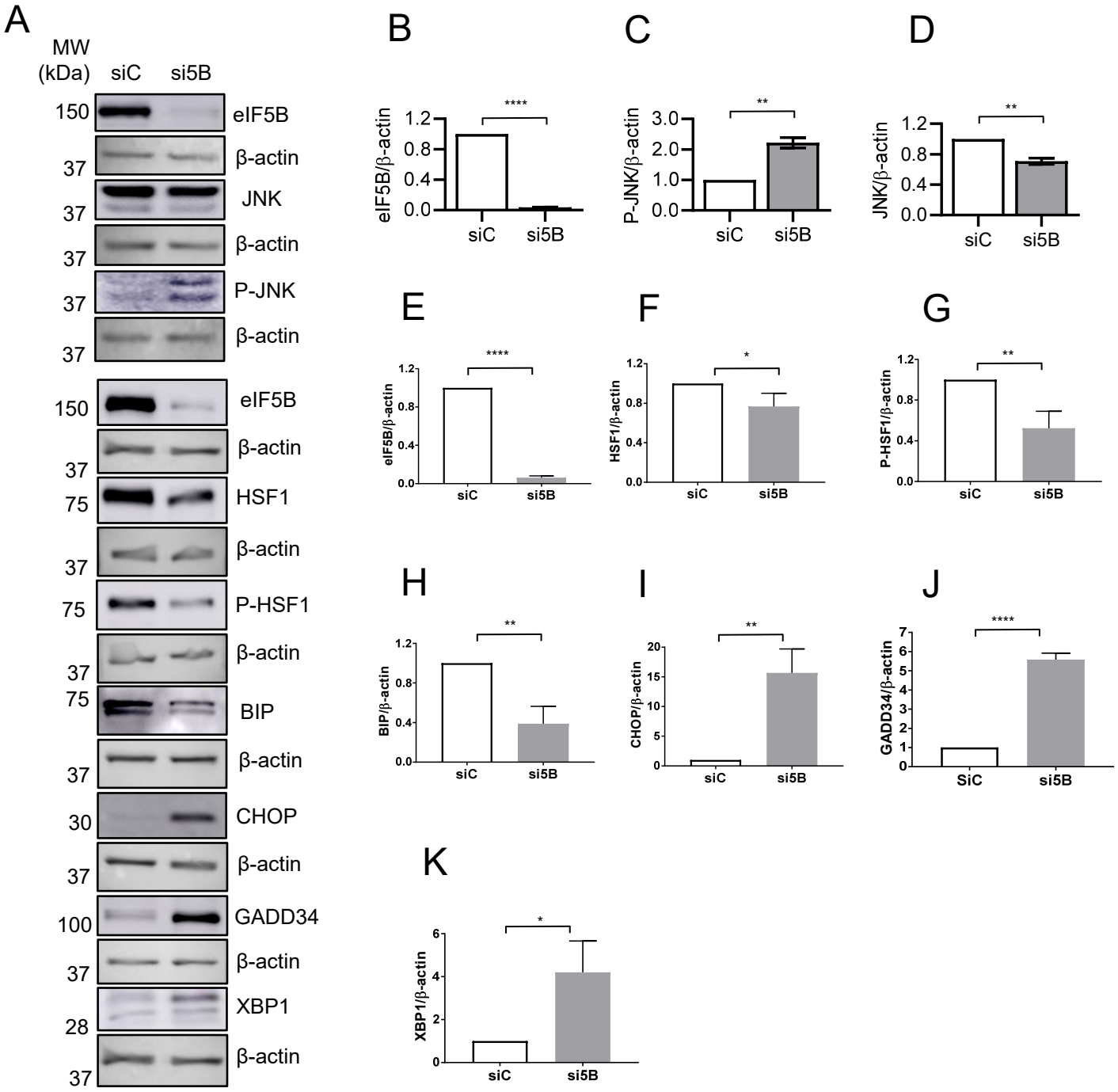
A
MW (kDa)
siC
si5B
150
eIF5B
β-actin
37
JNK
37
β-actin
37
P-JNK
37
β-actin
37
150
eIF5B
β-actin
37
75
HSF1
β-actin
37
75
P-HSF1
β-actin
37
75
BIP
β-actin
37
30
CHOP
β-actin
37
100
GADD34
β-actin
37
28
XBP1
β-actin
37
B
eIF5B/β-actin
1.2
0.8
0.4
0.0
****
siC
si5B
C
P-JNK/β-actin
3.0
2.0
1.0
0.0
**
siC
si5B
D
JNK/β-actin
1.2
0.8
0.4
0.0
**
siC
si5B
E
eIF5B/β-actin
1.2
0.8
0.4
0.0
****
siC
si5B
F
HSF1/β-actin
1.2
0.8
0.4
0.0
*
siC
si5B
G
P-HSF1/β-actin
1.2
0.8
0.4
0.0
**
siC
si5B
H
BIP/β-actin
1.2
0.8
0.4
0.0
**
siC
si5B
I
CHOP/β-actin
20
15
10
5
0
**
siC
si5B
J
GADD34/β-actin
7
6
5
4
3
2
1
0
****
SiC
si5B
K
XBP1/β-actin
6
4
2
0
*
siC
si5B

A

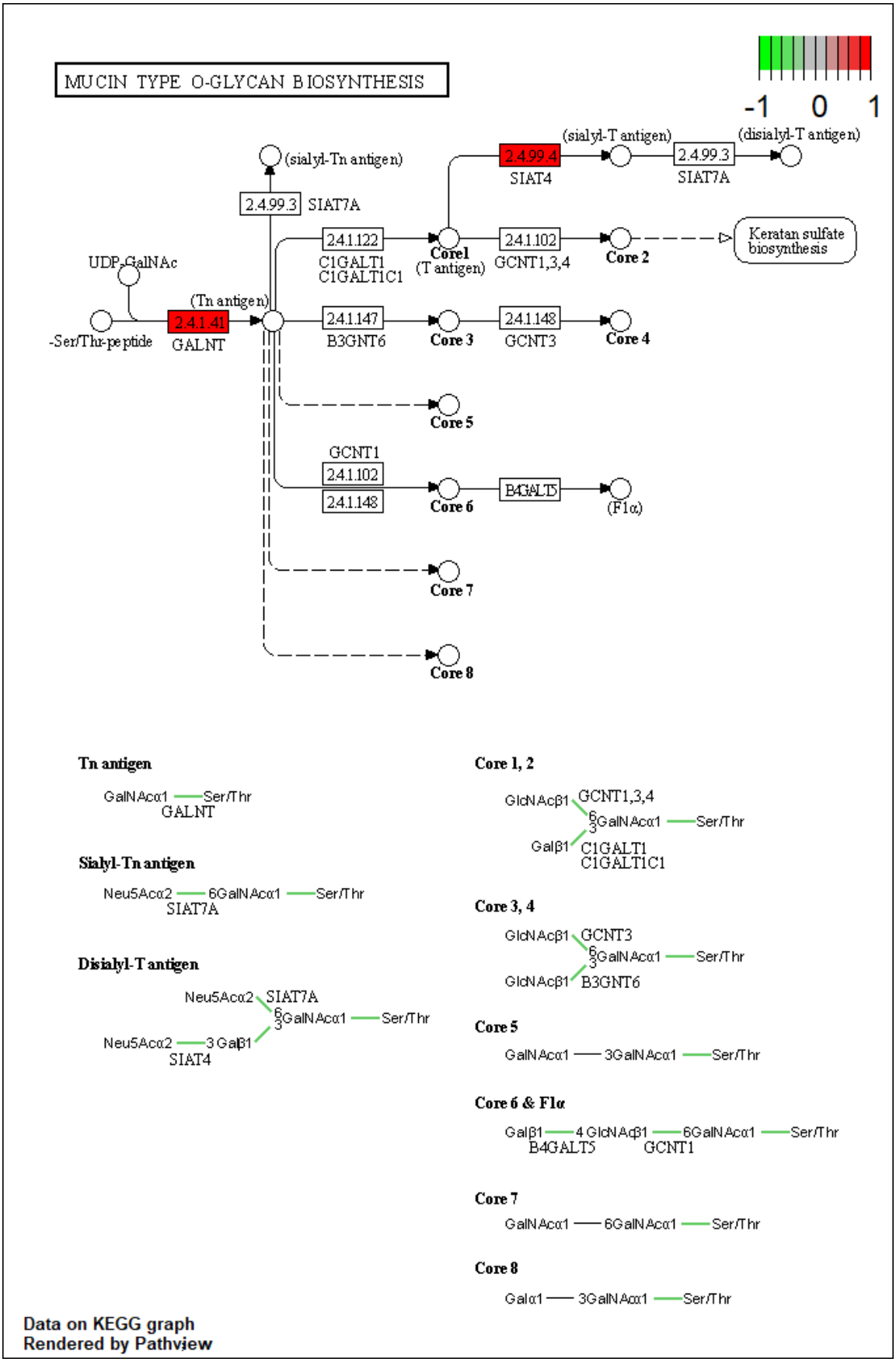
MUCIN TYPE O-GLYCAN BIOSYNTHESIS
-1 0 1
(sialyl-Tn antigen)
2.4.99.3 SIAT7A
2.4.99.4 SIAT4
(sialyl-T antigen)
2.4.99.3 SIAT7A
(disialyl-T antigen)
UDP-GalNAc
-Ser/Thr-peptide
2.4.1.41 GALNT
(Tn antigen)
2.4.1.122 C1GALT1 C1GALT1C1
Core1 (T antigen)
2.4.1.102 GCNT1,3,4
Core 2
Keratan sulfate biosynthesis
2.4.1.147 B3GNT6
Core 3
2.4.1.148 GCNT3
Core 4
Core 5
GCNT1
2.4.1.102
2.4.1.148
Core 6
B4GALT5
(F1α)
Core 7
Core 8
Tn antigen
GalNAcα1 Ser/Thr
GALNT
Sialyl-Tn antigen
Neu5Acα2 6GalNAcα1 Ser/Thr
SIAT7A
Disialyl-T antigen
Neu5Acα2 SIAT7A
6
3
GalNAcα1 Ser/Thr
Neu5Acα2 3 Galβ1
SIAT4
Core 1, 2
GlcNAcβ1 GCNT1,3,4
6
3
GalNAcα1 Ser/Thr
Galβ1 C1GALT1
C1GALT1C1
Core 3, 4
GlcNAcβ1 GCNT3
6
3
GalNAcα1 Ser/Thr
GlcNAcβ1 B3GNT6
Core 5
GalNAcα1 3GalNAcα1 Ser/Thr
Core 6 & F1α
Galβ1 4 GlcNAcβ1 6GalNAcα1 Ser/Thr
B4GALT5 GCNT1
Core 7
GalNAcα1 6GalNAcα1 Ser/Thr
Core 8
Galα1 3GalNAcα1 Ser/Thr
Data on KEGG graph
Rendered by Pathview

B

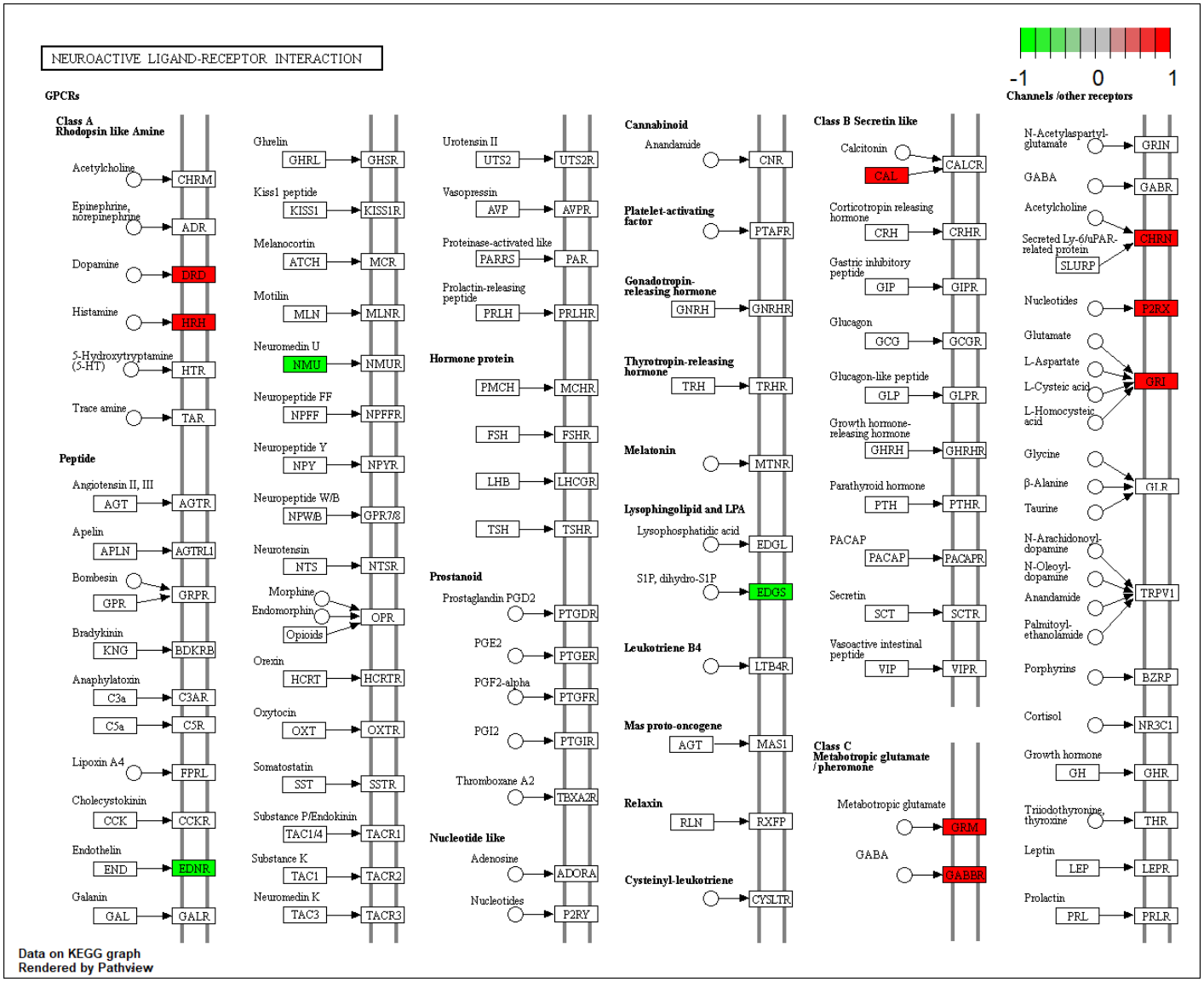
NEUROACTIVE LIGAND-RECEPTOR INTERACTION
-1
0
1
GPCRs
Class A Rhodopsin like Amine
Acetylcholine
CHRM
Epinephrine, norepinephrine
ADR
Dopamine
DRD
Histamine
HRH
5-Hydroxytryptamine (5-HT)
HTR
Trace amine
TAR
Peptide
Angiotensin II, III
AGT
AGTR
Apelin
APLN
AGTRL1
Bombesin
GPR
GRPR
Bradykinin
KNG
BDKRB
Anaphylatoxin
C3a
C3AR
C5a
C5R
Lipoxin A4
FPRL
Cholecystokinin
CCK
CCKR
Endothelin
END
EDNR
Galanin
GAL
GALR
Ghrelin
GHRL
GHSR
Kiss1 peptide
KISS1
KISS1R
Melanocortin
ATCH
MCR
Motilin
MLN
MLNR
Neuromedin U
NMU
NMUR
Neuropeptide FF
NPFF
NPFFR
Neuropeptide Y
NPY
NPYR
Neuropeptide W/B
NPW/B
GPR7/8
Neurotensin
NTS
NTSR
Morphine
Endomorphin
Opioids
OPR
Orexin
HCRT
HCRTR
Oxytocin
OXT
OXTR
Somatostatin
SST
SSTR
Substance P/Endokinin
TAC1/4
TACR1
Substance K
TAC1
TACR2
Neuromedin K
TAC3
TACR3
Urotensin II
UTS2
UTS2R
Vasopressin
AVP
AVPR
Proteinase-activated like
PARRS
PAR
Prolactin-releasing peptide
PRLH
PRLHR
Hormone protein
PMCH
MCHR
FSH
FSHR
LHB
LHCGR
TSH
TSHR
Prostanoid
Prostaglandin PGD2
PTGDR
PGE2
PTGER
PGF2-alpha
PTGFR
PGI2
PTGIR
Thromboxane A2
TBXA2R
Nucleotide like
Adenosine
ADORA
Nucleotides
P2RY
Cannabinoid
Anandamide
CNR
Platelet-activating factor
PTAFR
Gonadotropin-releasing hormone
GNRH
GNRHR
Thyrotropin-releasing hormone
TRH
TRHR
Melatonin
MTNR
Lysophingolipid and LPA
Lysophosphatidic acid
EDGL
S1P, dihydro-S1P
EDGS
Leukotriene B4
LTB4R
Mas proto-oncogene
AGT
MAS1
Relaxin
RLN
RXFP
Cysteinyl-leukotriene
CYSLTR
Class B Secretin like
Calcitonin
CAL
CALCR
Corticotropin releasing hormone
CRH
CRHR
Gastric inhibitory peptide
GIP
GIPR
Glucagon
GCG
GCGR
Glucagon-like peptide
GLP
GLPR
Growth hormone-releasing hormone
GHRH
GHRHR
Parathyroid hormone
PTH
PTHR
PACAP
PACAP
PACAPR
Secretin
SCT
SCTR
Vasoactive intestinal peptide
VIP
VIPR
Class C Metabotropic glutamate /pheromone
Metabotropic glutamate
GRM
GABA
GABBR
Channels /other receptors
N-Acetylaspartyl-glutamate
GRIN
GABA
GABR
Acetylcholine
Secreted Ly-6/uPAR-related protein
SLURP
CHRN
Nucleotides
P2RX
Glutamate
L-Aspartate
L-Cysteic acid
L-Homocysteic acid
GRI
Glycine
β-Alanine
Taurine
GLR
N-Arachidonoyl-dopamine
N-Oleoyl-dopamine
Anandamide
Palmitoyl-ethanolamide
TRPV1
Porphyrins
BZRP
Cortisol
NR3C1
Growth hormone
GH
GHR
Triiodothyronine, thyroxine
THR
Leptin
LEP
LEPR
Prolactin
PRL
PRLR
Data on KEGG graph
Rendered by Pathview

C

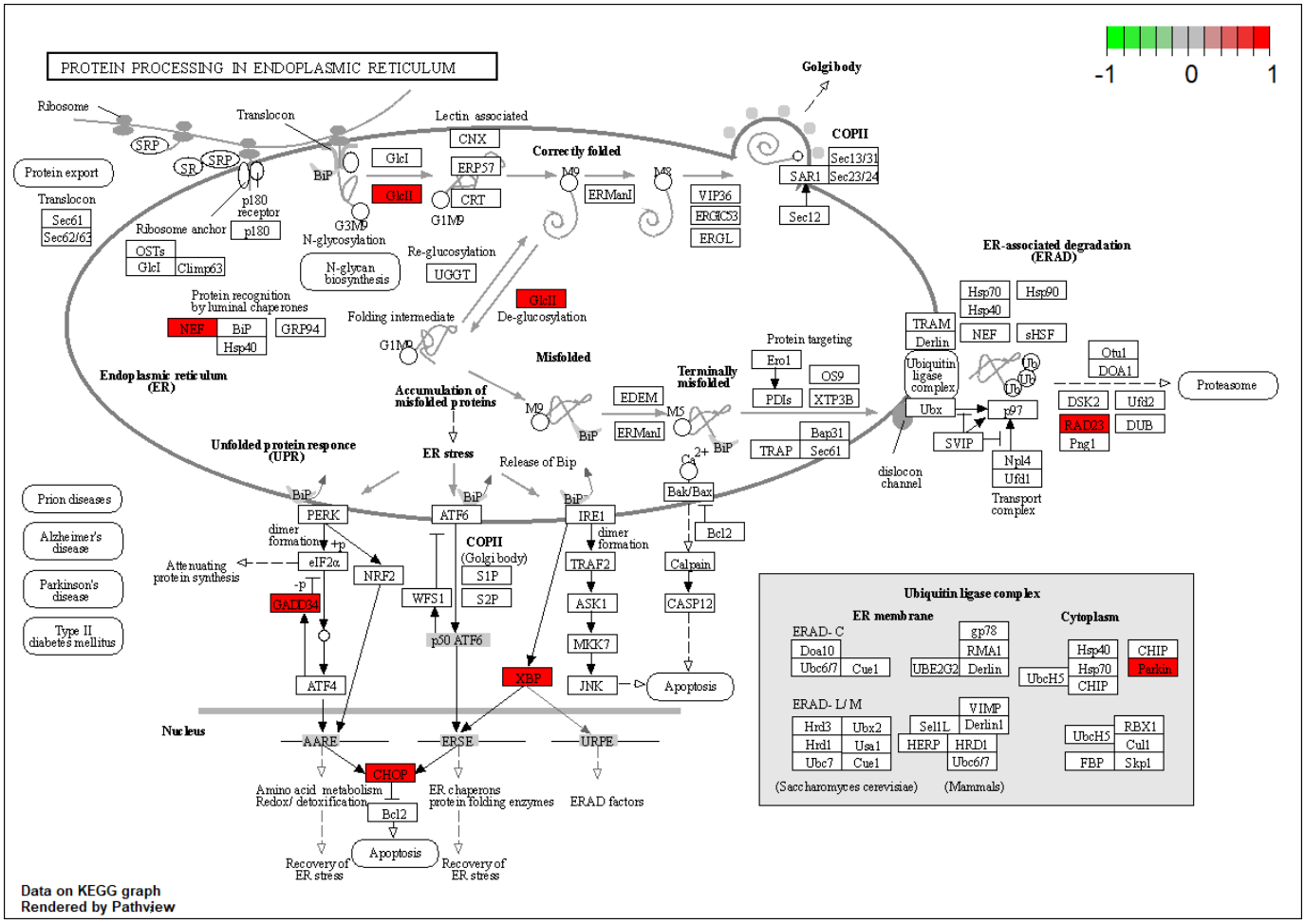
PROTEIN PROCESSING IN ENDOPLASMIC RETICULUM
-1
0
1
Golgi body
Ribosome
Translocon
Lectin associated
CNX
COPII
Sec13/31
Sec23/24
SAR1
Sec12
Protein export
SRP
SR
Translocon
Sec61
Sec62/63
p180 receptor
Ribosome anchor
p180
OSTs
Glcl
Climp63
BiP
Glcl
GlcII
ERP57
CRT
G3M9
G1M9
N-glycosylation
N-glycan biosynthesis
Re-glucosylation
UGGT
Correctly folded
M9
ERManI
M8
VIP36
ERGIC53
ERGL
ER-associated degradation (ERAD)
Protein recognition by luminal chaperones
NEF
BiP
Hsp40
GRP94
Folding intermediate
De-glucosylation
GlcII
G1M9
Misfolded
Endoplasmic reticulum (ER)
Accumulation of misfolded proteins
EDEM
M9
M5
BiP
ERManI
Terminally misfolded
Protein targeting
Ero1
PDIs
OS9
XTP3B
Bap31
TRAP
Sec61
TRAM
Derlin
Ubiquitin ligase complex
Ub
Ubx
p97
SVIP
Npl4
Ufd1
Transport complex
dislocon channel
Hsp70
Hsp40
Hsp90
NEF
sHSF
Otu1
DOA1
DSK2
Ufd2
RAD23
DUB
Png1
Proteasome
Unfolded protein responce (UPR)
ER stress
Release of Bip
Ca 2+
Bak/Bax
Bcl2
Calpain
CASP12
Apoptosis
PERK
ATF6
IRE1
dimer formation
+p
eIF2α
-p
Attenuating protein synthesis
NRF2
GADD34
ATF4
COPII
(Golgi body)
S1P
S2P
WFS1
p50 ATF6
XBP
TRAF2
ASK1
MKK7
JNK
Prion diseases
Alzheimer's disease
Parkinson's disease
Type II diabetes mellitus
Nucleus
AARE
ERSE
URPE
CHOP
Amino acid metabolism
Redox/ detoxification
ER chaperons
protein folding enzymes
ERAD factors
Bcl2
Apoptosis
Recovery of ER stress
Recovery of ER stress
Ubiquitin ligase complex
ER membrane
Cytoplasm
ERAD- C
Doa10
Ubc6/7
Cue1
gp78
RMA1
UBE2G2
Derlin
UbcH5
Hsp40
Hsp70
CHIP
CHIP
Parkin
ERAD- L/ M
Hrd3
Ubx2
Hrd1
Usa1
Ubc7
Cue1
VIMP
Sel1L
Derlin1
HERP
HRD1
Ubc6/7
UbcH5
RBX1
Cul1
FBP
Skp1
(Saccharomyces cerevisiae)
(Mammals)
Data on KEGG graph
Rendered by Pathview

D

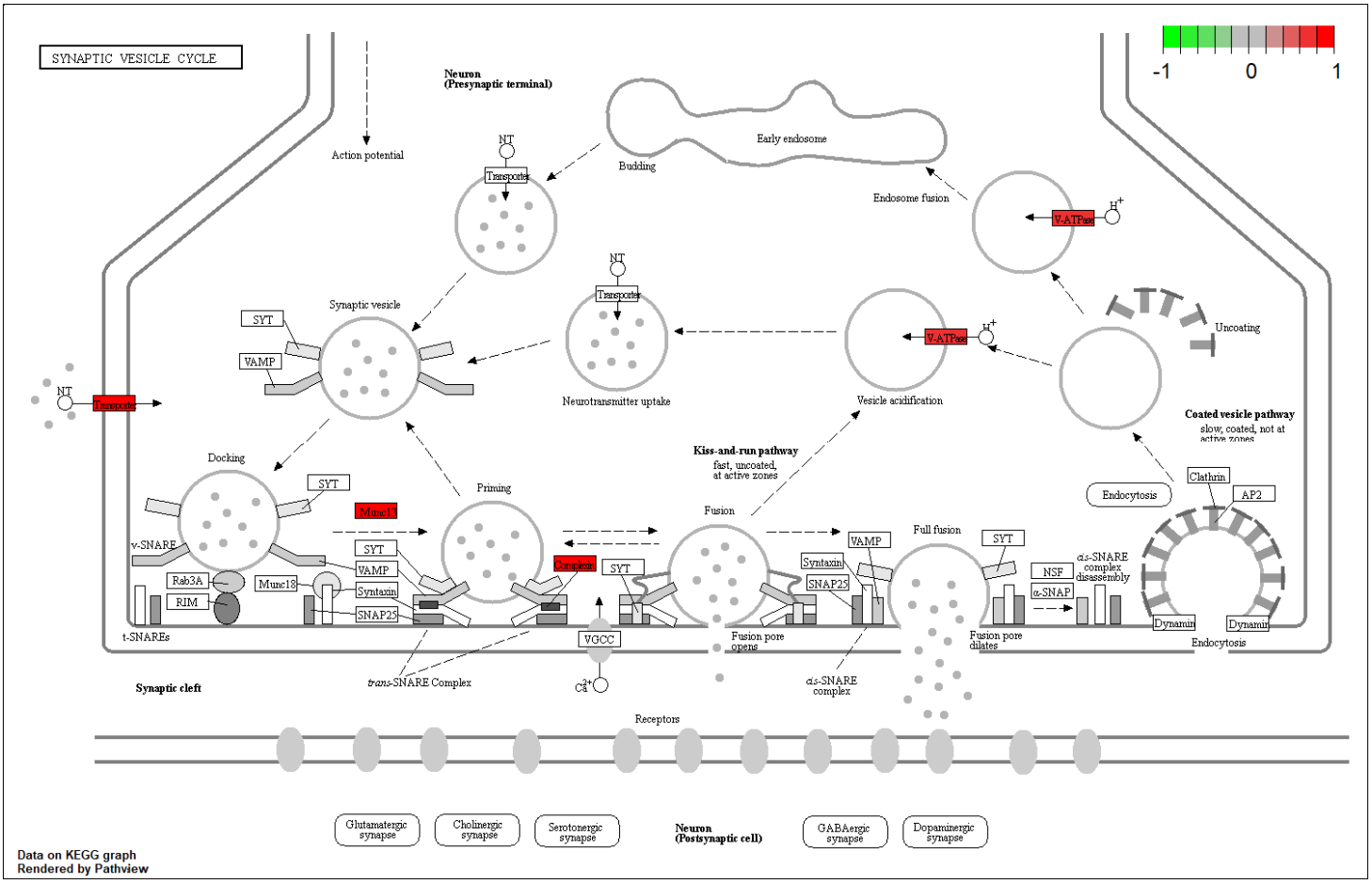
SYNAPTIC VESICLE CYCLE
-1
0
1
Neuron
(Presynaptic terminal)
Action potential
NT
Transporter
Budding
Early endosome
Endosome fusion
V-ATPase
H+
Synaptic vesicle
SYT
VAMP
Neurotransmitter uptake
Vesicle acidification
Uncoating
Coated vesicle pathway
slow, coated, not at active zones
Docking
Priming
Kiss-and-run pathway
fast, uncoated, at active zones
Fusion
Munc13
v-SNARE
Rab3A
RIM
Munc18
Syntaxin
SNAP25
Complexin
VAMP
Full fusion
NSF
α-SNAP
cis-SNARE complex disassembly
Clathrin
AP2
Endocytosis
Dynamin
t-SNAREs
Synaptic cleft
trans-SNARE Complex
VGCC
Ca2+
Fusion pore opens
Fusion pore dilates
cis-SNARE complex
Receptors
Glutamatergic synapse
Cholinergic synapse
Serotonergic synapse
Neuron
(Postsynaptic cell)
GABAergic synapse
Dopaminergic synapse
Data on KEGG graph
Rendered by Pathview

E

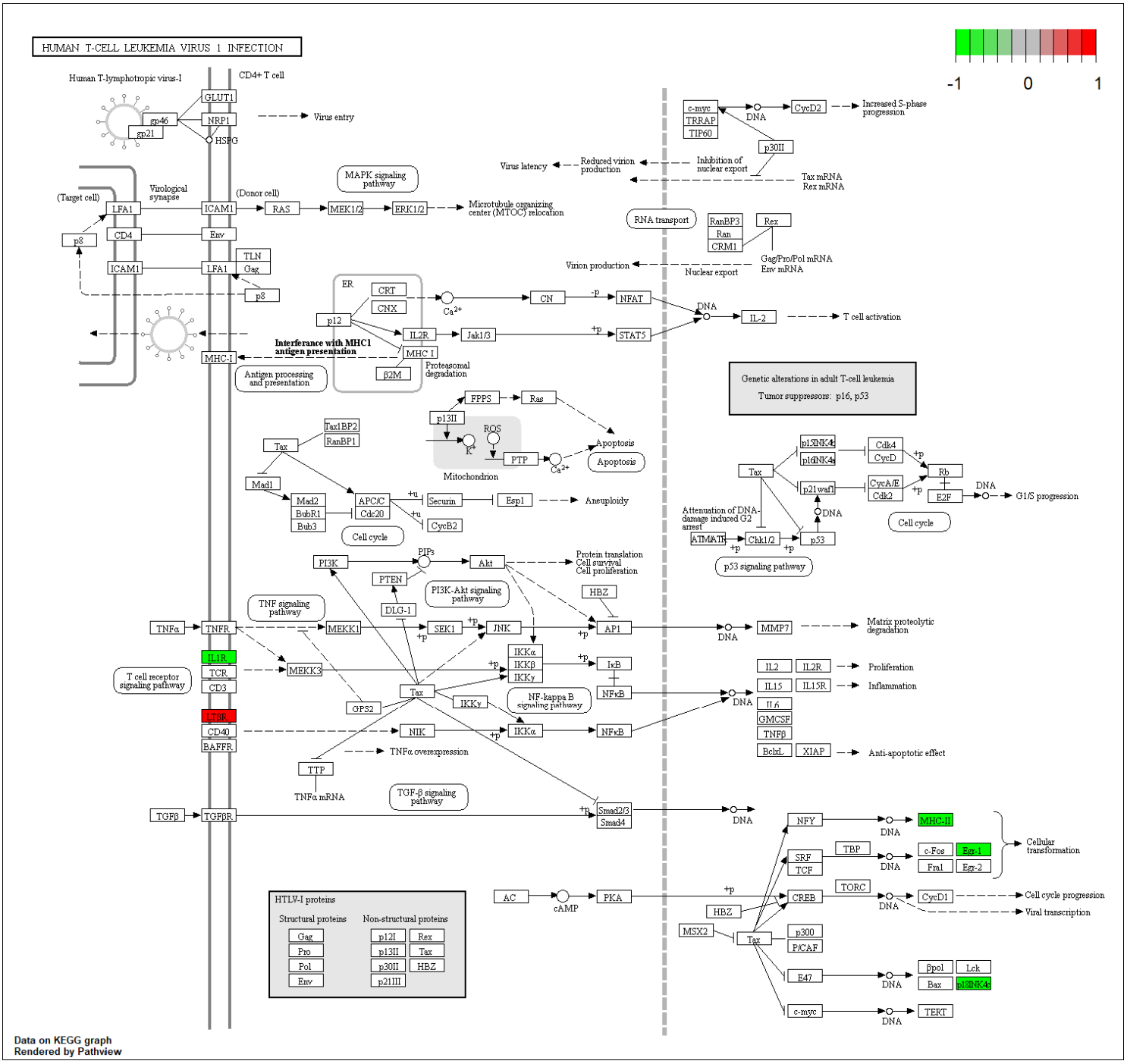
HUMAN T-CELL LEUKEMIA VIRUS 1 INFECTION
-1
0
1
Human T-lymphotropic virus-I
CD4+ T cell
GLUT1
gp46
gp21
NRP1
HSPG
Virus entry
(Target cell)
Virological synapse
(Donor cell)
LFA1
ICAM1
CD4
Env
p8
TLN
Gag
MAPK signaling pathway
RAS
MEK1/2
ERK1/2
Microtubule organizing center (MTOC) relocation
Interferance with MHC1 antigen presentation
MHC-I
Antigen processing and presentation
ER
CRT
CNX
p12
Ca2+
CN
NFAT
IL2R
Jak1/3
STAT5
MHC I
β2M
Proteasomal degradation
DNA
IL-2
T cell activation
c-myc
TRRAP
TIP60
CycD2
Increased S-phase progression
p30II
Virus latency
Reduced virion production
Inhibition of nuclear export
Tax mRNA
Rex mRNA
RNA transport
RanBP3
Ran
CRM1
Rex
Virion production
Nuclear export
Gag/Pro/Pol mRNA
Env mRNA
Genetic alterations in adult T-cell leukemia
Tumor suppressors: p16, p53
FPPS
Ras
p13II
ROS
K+
PTP
Ca2+
Apoptosis
Mitochondrion
Tax1BP2
RanBP1
Tax
Mad1
Mad2
BubR1
Bub3
APC/C
Cdc20
Securin
Esp1
Aneuploidy
CycB2
Cell cycle
p15INK4b
p16INK4a
Cdk4
CycD
CycA/E
Cdk2
Rb
E2F
G1/S progression
p21waf1
Attenuation of DNA-damage induced G2 arrest
ATM/ATR
Chk1/2
p53
p53 signaling pathway
PI3K
PIP3
Akt
PTEN
PI3K-Akt signaling pathway
Protein translation
Cell survival
Cell proliferation
HBZ
TNF signaling pathway
DLG-1
TNFα
TNFR
MEKK1
SEK1
JNK
AP1
MMP7
Matrix proteolytic degradation
IL1R
TCR
CD3
T cell receptor signaling pathway
MEKK3
LTβR
CD40
BAFFR
GFS2
IKKα
IKKβ
IKKγ
IκB
NFκB
NF-kappa B signaling pathway
NIK
TNFα overexpression
TTP
TNFα mRNA
IL2
IL2R
Proliferation
IL15
IL15R
Inflammation
IL6
GMCSF
TNFβ
BclxL
XIAP
Anti-apoptotic effect
TGF-β signaling pathway
TGFβ
TGFβR
Smad2/3
Smad4
NFY
MHC-II
SRF
TCF
TBP
c-Fos
Fra1
Egr-1
Egr-2
Cellular transformation
AC
cAMP
PKA
TORC
CREB
CycD1
Cell cycle progression
Viral transcription
MSX2
p300
P/CAF
E47
βpol
Bax
Lck
p18INK4c
c-myc
TERT
HTLV-I proteins
Structural proteins
Gag
Pro
Pol
Env
Non-structural proteins
p12I
p13II
p30II
p21III
Rex
Tax
HBZ
Data on KEGG graph
Rendered by Pathview

F

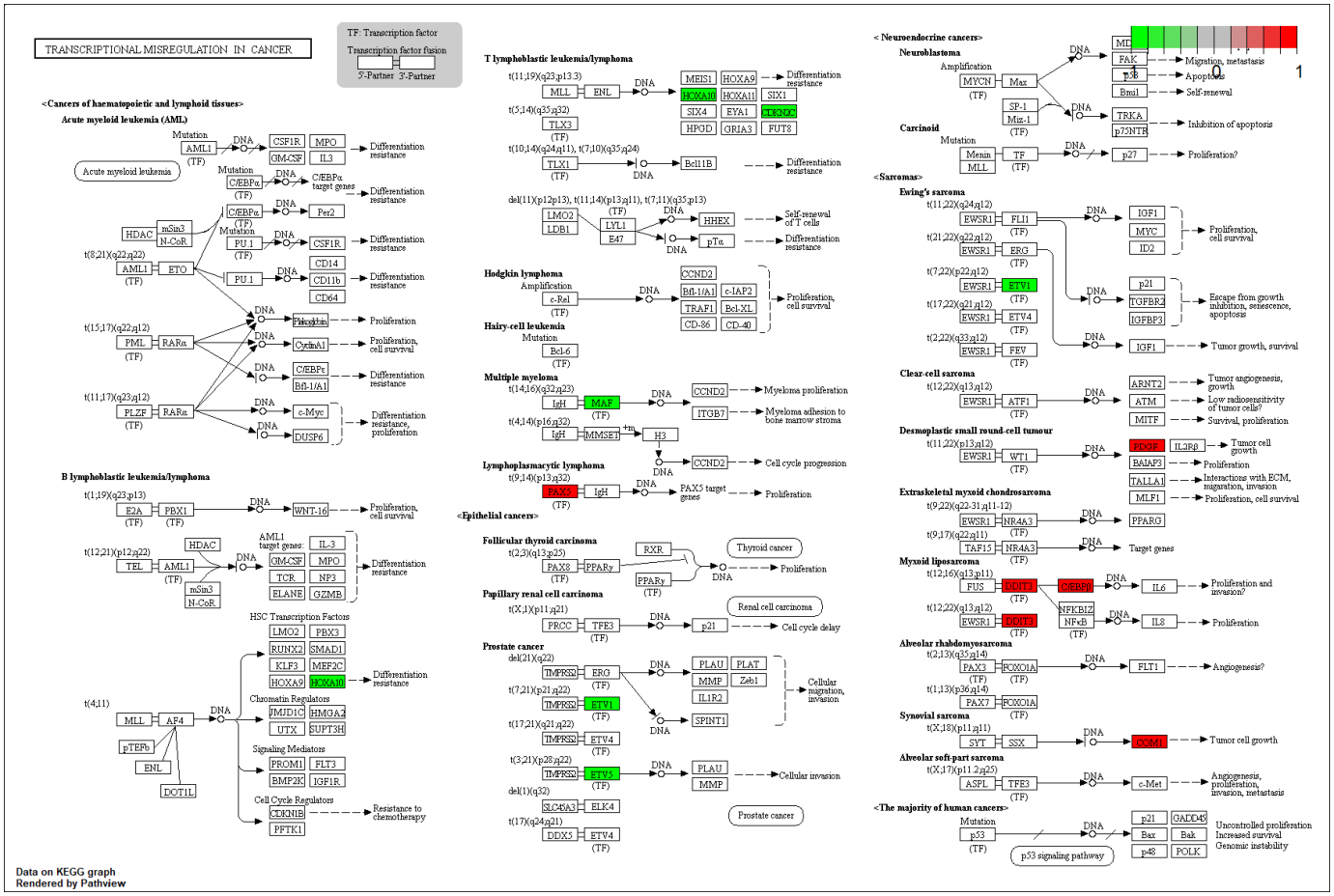

Figure S1. Significantly upregulated **(A-D)** and downregulated **(E-F)** KEGG pathways upon eIF5B depletion.

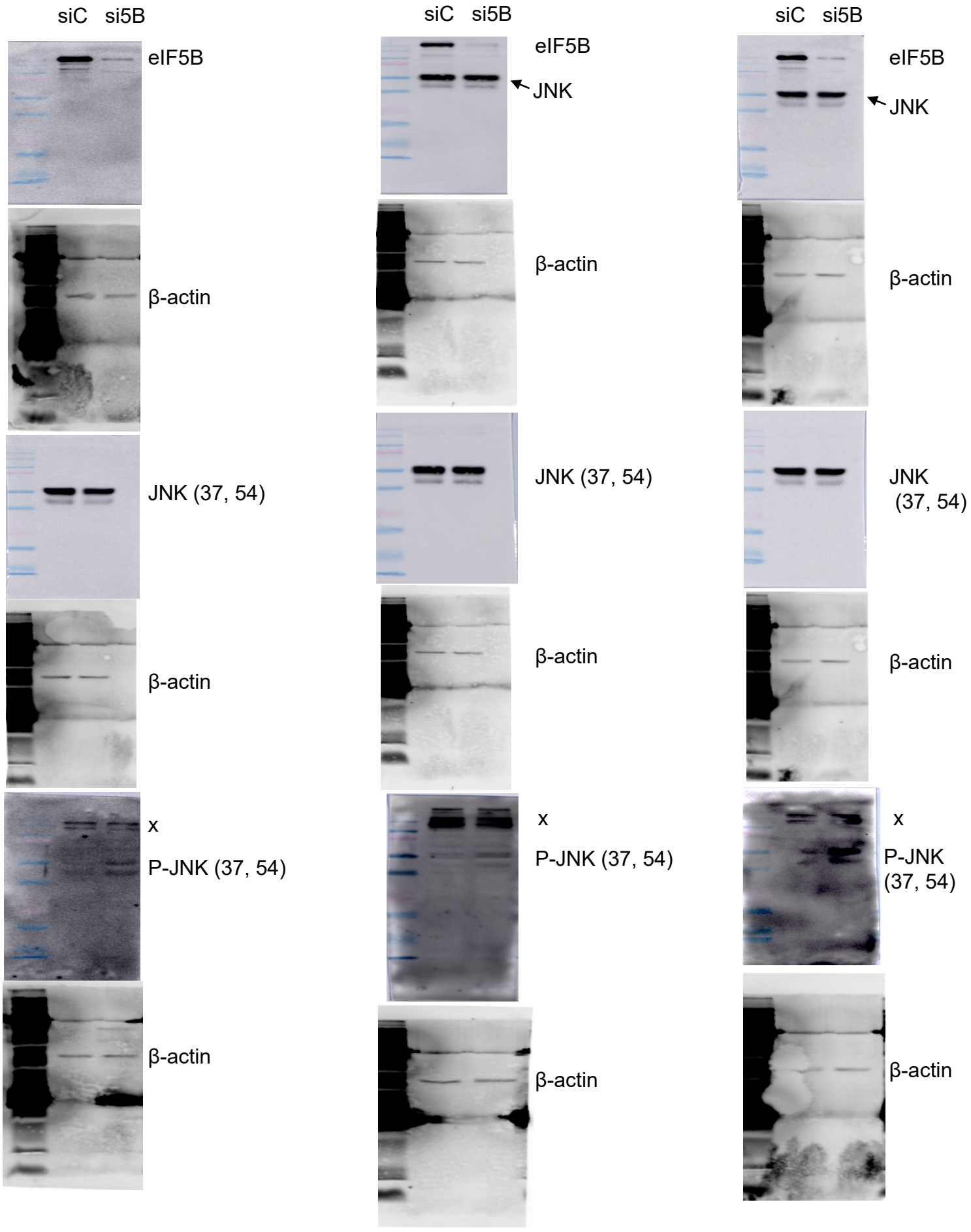
siC si5B
eIF5B
β-actin
JNK (37, 54)
β-actin
x
P-JNK (37, 54)
β-actin
siC si5B
eIF5B
JNK
β-actin
JNK (37, 54)
β-actin
x
P-JNK (37, 54)
β-actin
siC si5B
eIF5B
JNK
β-actin
JNK
(37, 54)
β-actin
x
P-JNK
(37, 54)
β-actin

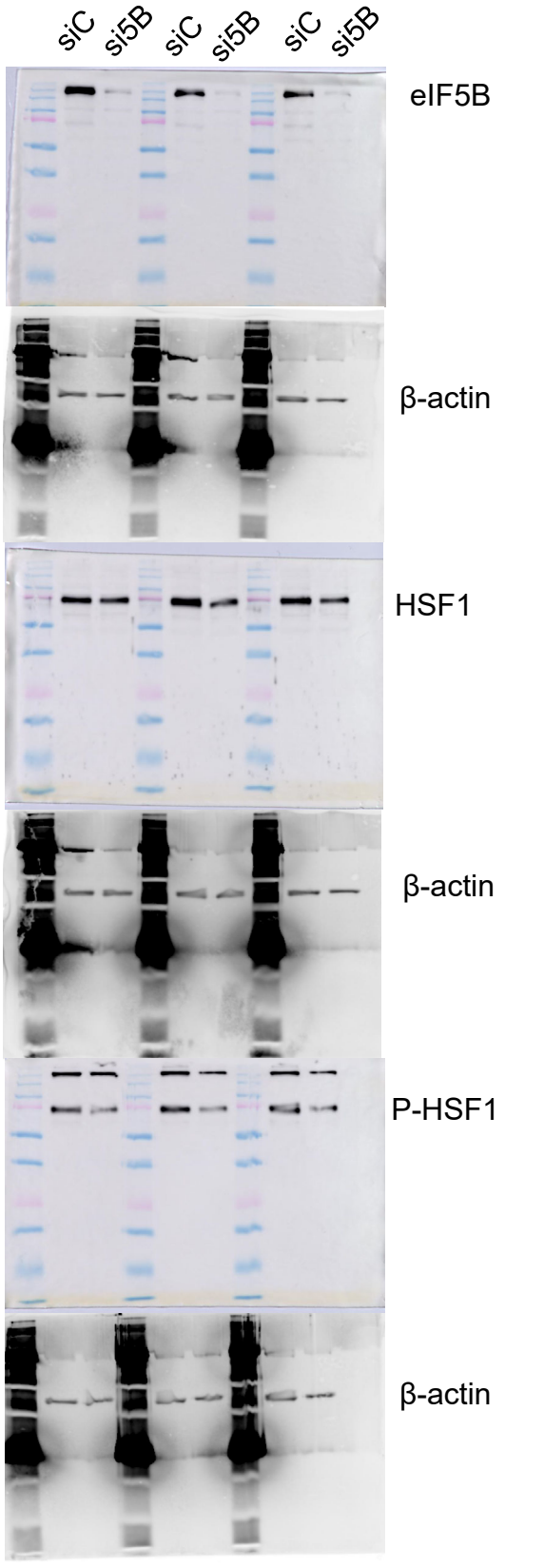
siC
si5B
siC
si5B
siC
si5B
eIF5B
β-actin
HSF1
β-actin
P-HSF1
β-actin

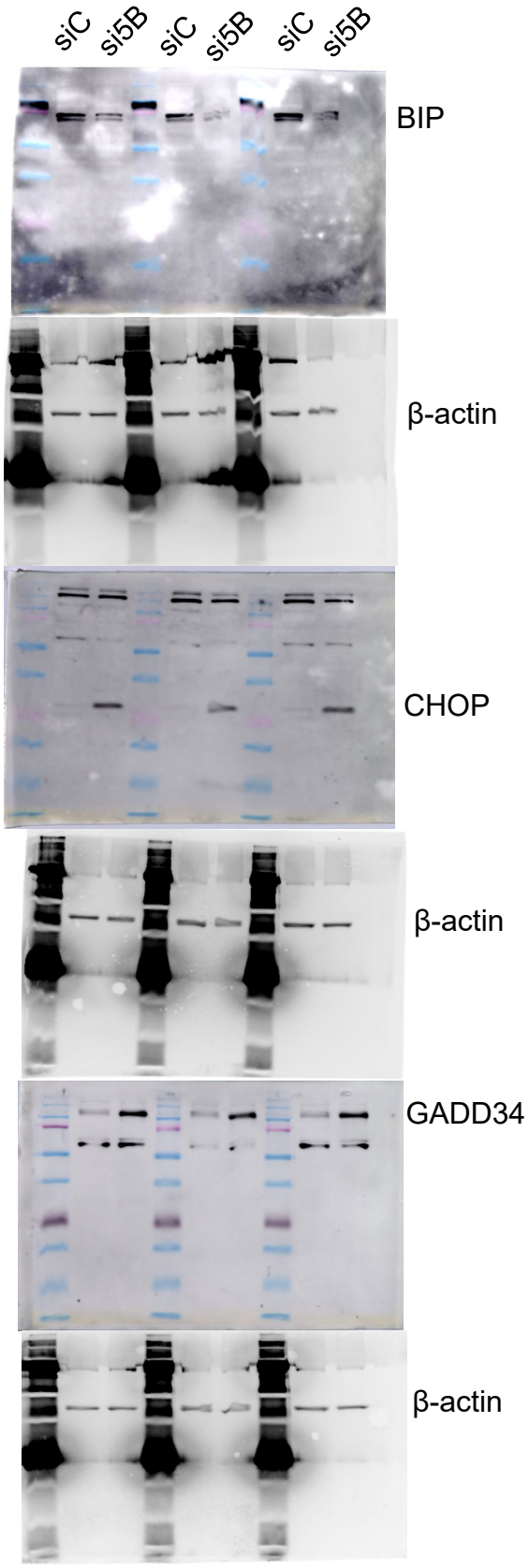
siC
si5B
siC
si5B
siC
si5B
BIP
β-actin
CHOP
β-actin
GADD34
β-actin

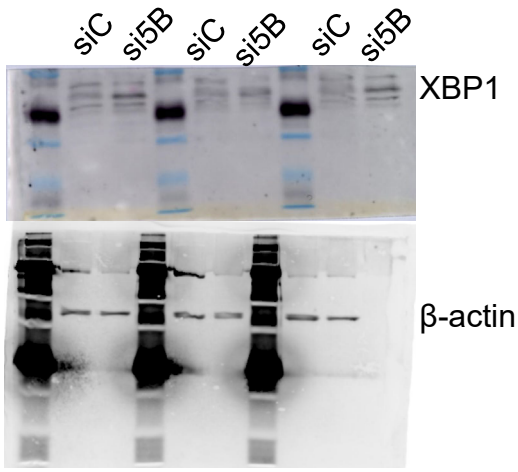

Figure S2. Depletion of eIF5B leads to activation of ER stress and increased levels of the phosphorylated JNK protein in HEK 293T cells. HEK 293T cells were transfected with a non-specific control siRNA (siC) or an eIF5B-specific siRNA pool (si5B) and resolved by SDS-PAGE before performing immunoblotting. Original, full-length biological triplicate Western blots for eIF5B, total JNK (P54 and P46), phospho-JNK (P54 and P46), HSF1, phosphor-HSF1, BIP, CHOP, GADD34, XBP1 and β-actin (internal control). Representative images were cropped and shown in Figure 3. Note that total two of the JNK blots were re-probed with anti-eIF5B antibody; the JNK bands are indicated with an arrow. Note also that, for P-JNK, a cross-reactive species (x) was observed for all replicates, the levels of which appeared to match those of β-actin.

List of antibodies used:

Protein	Antibody Company	Antibody Catalogue #
eIF5B	Protein Tech	13527-1-AP
JNK	Cell Signaling Tech	9252
P-JNK	Cell Signaling Tech	9251
HSF1	Enzo	ADI-SPA-901
P-HSF1	Invitrogen	PA5-101018
BIP	Protein Tech	11587-1-AP
CHOP	Protein Tech	15204-1-AP
GADD34	Protein Tech	10449-1-AP
XBP1	Protein Tech	24168-1-AP
Actin (hFAB Rhodamine)	BioRad	12004163
Secondary antibody: Goat anti-rabbit-HRP Conjugate	Abcam	Ab97051